Dilution drives deep degassing of sulfur in hydrous magmas

Ery C. Hughes: University College London (ery.hughes@ucl.ac.uk)
Edward M. Stolper: Caltech

This pre-print is not an accepted peer-reviewed manuscript. A version of this pre-print has been submitted to Journal of Petrology for peer-review.

Dilution drives deep degassing of sulfur in hydrous magmas

Ery C. Hughes[1,2*] and Edward M. Stolper[3]

1 Department of Earth Sciences, University College London, London, WC1E 6BS, UK

2 National Isotope Centre, Earth Sciences New Zealand, Gracefield, 5010, Aotearoa New Zealand

3 Division of Geological and Planetary Sciences, Caltech, Pasadena, 91101, California USA

*corresponding author: ery.hughes@ucl.ac.uk

ECH: 0000-0002-3445-281X

EMS: 0000-0001-8008-8804

Abstract

Sulfur (S) is thought to degas deep from hydrous magmas (e.g., arc basalts), in contrast to water-poor magmas where S degasses at very shallow depths (e.g., Kīlauea, mid-ocean ridge basalts). Our modelling of degassing shows this occurs for magmas that are both reduced (i.e., S is present predominantly as H_2S in the vapor and dissolved sulfide in the melt) and oxidised (i.e., SO_2 in the vapor and dissolved sulfate in the melt). Even deeper degassing occurs for silicate melts containing both dissolved sulfide and sulfate due to the sulfur solubility minimum. Additionally, deep degassing of a fictive, inert, and ideal gas species that behaves like a noble gas but with a similar solubility to S occurs in hydrous magmas. We show that dilution by additional gas species (i.e., H_2O and CO_2) in the vapor phase is the main driver of deep degassing of S, which can be further enhanced for magmas at the sulfur solubility minimum. Dilution is the same effect that drives deeper degassing of H_2O and CO_2 in melts containing both compared to pure-H_2O or -CO_2; deep degassing of H_2O or He in CO_2-rich systems; and reduces the S content in gases during hydrous degassing. This mechanism does not require a direct effect of H_2O (or CO_2) on the solubility of S, although H_2O does decrease the solubility of S, contributing to the deep degassing of S. The dilution effect impacts all volatile species, with its magnitude depending on the relative solubilities and concentrations of the different volatiles present.

Keywords: degassing; dilution; magma; sulfur; water

Introduction

Sulfur (S) is often the third most abundant volatile element in undegassed terrestrial magmas after H_2O and CO_2, such that S-bearing species are important constituents of volcanic gasses (e.g., Metrich & Mandeville, 2010; Wallace, 2005; Wallace & Edmonds, 2011). Sulfur has been inferred to begin to degas significantly from mid-ocean ridge (MORB) and Hawaiian basaltic magmas on ascent at much lower pressure (*P*, ~200–300 MPa) than CO_2 and at *P*'s comparable to those at which H_2O degasses significantly based on analyses of submarine glass and melt/fluid inclusions (e.g., Dixon et al., 1991; Lerner et al., 2021; Moore & Clague, 1987; Moore & Fabbi, 1971; Moore & Schilling, 1973; Moore & Thomas, 1988; Moussallam et al., 2016; Wallace & Carmichael, 1992; Wallace & Edmonds, 2011; Wieser et al., 2025). This behaviour has been attributed to the typically relatively low (and similar) concentrations of S and H_2O (~0.1–0.8 wt.%) and their relatively high (and similar) solubilities in these magmas, especially compared to CO_2. However, these observations contrast with measurements in some island arc and back arc basin basalts from submarine lavas (e.g., Brounce et al., 2016; Davis et al., 1991; Nilsson & Peach, 1993) and melt inclusions that have quantified the CO_2 contents of melt-inclusion-hosted bubbles (e.g., Rasmussen et al., 2020), that have low S contents at relatively high *P* despite similar initial S contents to MORB and Hawai'i (~0.1–0.3 wt.%); and analysis at Mauna Loa (Hawai'i) that detect significant amounts of SO_2 in relatively high-density-CO_2 fluid inclusions (Wieser et al., 2025). These observations suggest that there can be significant degassing of S – even roughly concurrently with CO_2 in the melt inclusions – at relatively high *P*. Additionally, such deeply degassed S has been invoked as the source of S-bearing gases found in evolved, shallower magmas and thereby to explain the "excess sulfur problem" (e.g., Christopher et al., 2010; Di Muro et al., 2008; Edmonds et al., 2010; Pallister et al., 1992; Roberge et al., 2009; Wallace, 2001) and as a potential trigger for precipitation of sulfide ores in porphyry

copper deposits (e.g., Blundy et al., 2015; Hattori & Keith, 2001). This degassing behaviour of S from arc magmas is consistent with degassing models of water-rich magmas as they ascend, which predict that at the same bulk S content, S begins to degas much deeper from water-rich magmas than from water-poor magmas (e.g., Boulliung & Wood, 2022; Ding et al., 2023; Edmonds & Wallace, 2017; Wallace & Edmonds, 2011; Yip et al., 2022). For Mauna Loa, deeper degassing of S agrees with modelling that has higher initial S^{6+}/S_T (0.3–0.4) than required for Kīlauea (0.1–0.2; Wieser et al., 2025).

Most explanations for the deeper degassing of S in hydrous magmas relate to changes in the partition coefficient (alternatively referred to as the equilibrium constant) of S between melt and vapor such that S transfers from the melt to the vapor at higher *P* in hydrous magmas compared to water-poor magmas, including: (1) a direct effect of H_2O on the partition coefficient between dissolved sulfide and H_2S vapor (i.e., $\Delta FMQ < +0.5$; Ding et al., 2023 – FMQ is the oxygen fugacity (f_{O2}) of the Fayalite-Magnetite-Quartz buffer, and ΔFMQ is the difference in log units between the f_{O2} of the degassing magma and this buffer; e.g., Frost, 1991); (2) the effects of temperature (*T*), f_{O2}, or melt composition on the behaviour of S that are associated with magmas that are more likely to be hydrous (e.g., Métrich et al., 2009; Wallace & Edmonds, 2011; Zajacz et al., 2012); and (3) the lower total solubility of S at the sulfur solubility minimum (SS^{min}, due to the presence of both dissolved sulfide and sulfate in the melt) that occurs near ~ΔFMQ+1, which is close to f_{O2} values of typical arc magmas (e.g., Ding et al., 2023; Hughes, Saper, et al., 2023; Nilsson & Peach, 1993). Other explanations highlight that the partial degassing of S at high *P* could be related to the outgassing of other volatiles (e.g., CO_2 or H_2O; Davis et al., 1991; Dixon & Stolper, 1995; Wallace & Edmonds, 2011). For instance, even for the same partition coefficient of S, for a greater mass fraction of H_2O exsolved, there will be more S partitioned into the vapor (Wallace & Edmonds, 2011).

We apply *VolFe* (Hughes, Liggins, Wieser, et al., 2025) to model closed- and open-system degassing of a representative Hawaiian basaltic melt spanning a range of initial H_2O, CO_2, and S concentrations and initial values of f_{O2}. Our modelling largely agrees with previous modelling (e.g., Boulliung & Wood, 2022, 2023; Ding et al., 2023; Edmonds & Wallace, 2017; Gaillard & Scaillet, 2009; Wallace & Edmonds, 2011; Yip et al., 2022) in that during closed-system degassing the following are observed: (1) for relatively reduced magmas (initial $\Delta FMQ \lesssim 0$), S degasses at higher P for water-rich relative to water-poor melts; (2) this effect is positively correlated with the H_2O content of the system for a given initial f_{O2}; and (3) the magnitude of this effect is enhanced in the vicinity of the SS^{min}. However, we also show that this effect is observed for closed-system degassing of magmas more oxidizing than the SS^{min} (i.e., for conditions at which the concentration of H_2S is negligible in both melt and coexisting vapor) or when H_2S is forced artificially to be absent in the melt and/or vapor even under reducing conditions. It also occurs in our modelling for open-system degassing. Finally – and importantly – we show that this effect is also predicted for inert volatile components that are present in the vapor and melt as a single species (e.g., the noble gases). Consequently, the effect of dissolved H_2O on the P at which significant amounts of such a volatile component degasses cannot be attributed dominantly to the concentrations or specific behaviours of f_{O2}-sensitive species such as H_2S or to any structural or thermochemical factors unique to S-bearing magmas, although these do have some influence.

Based on numerical experiments we performed with *VolFe*, we conclude that these results can be understood via the "dilution effect" (e.g., O. E. Anderson et al., 2024, 2025; Dixon & Stolper, 1995; Gaillard & Scaillet, 2009; Gonnermann & Mukhopadhyay, 2007; Iacovino et al., 2021; Lowenstern, 2001; Webster & Botcharnikov, 2011). For instance, consider a simple melt-vapor system containing only H_2O at a given P, T, and silicate melt

composition. When the system contains both melt and vapor and the vapor is assumed to be pure H_2O, the vapor-saturated melt has a well-defined concentration of dissolved H_2O. If CO_2 is added to the system at constant *P* and *T*, some of it must partition into the vapor (and most of it will given its typically low solubility relative to H_2O; e.g., Dixon et al., 1995). The H_2O in the vapor is thereby *diluted* by the CO_2 in the vapor: i.e., the partial pressure and fugacity of H_2O (p_{H2O} and f_{H2O}) must decrease. Consequently (as H_2O dissolution roughly follows Seivert's law; e.g., Dixon et al., 1995; Stolper, 1982), the melt H_2O concentration must decrease when CO_2 is added to the system (e.g., Dixon & Stolper, 1995; Lowenstern, 1995), resulting in transfer (i.e., degassing) of H_2O from melt to vapor. Similarly, starting from a melt + vapor assemblage in a system in which CO_2 is the only volatile component, addition of H_2O dilutes the CO_2 in the vapor, resulting in CO_2 degassing from melt into vapor. The dilution effect has been applied to explain changes in the degassing behaviour of H_2O-CO_2 as their concentrations change (e.g., Anderson et al., 2024, 2025; Dixon & Stolper, 1995; Iacovino et al., 2021; Lowenstern, 2001) and the greater degree of degassing of He in CO_2-rich ocean island basalts (OIB) relative to MORBs (Gonnermann & Mukhopadhyay, 2007). Additionally, it has been invoked to explain the decreasing S content of volcanic gases with increased initial H_2O during degassing (Gaillard & Scaillet, 2009) and now we apply it to explaining the deep degassing of S in hydrous magmas (Dixon & Stolper, 1995).

The behaviour of sulfur during degassing

VolFe (v1.0) can be applied to modelling the behaviour of C-H-O-S-bearing volatile species during isothermal, equilibrium, closed- or open-system, decompression-induced degassing (Hughes, Liggins, Wieser, et al., 2025). As in Hughes et al. (2023, 2024a), all calculations presented in this paper use a single volatile-free melt composition (i.e., a

Hawaiian tholeiite from Brounce et al., 2017) at a T of 1200°C (Supplementary Table 1). Melt and vapor species considered and model options used in calculations presented in this paper are detailed in Supplementary Table S2. A Jupyter notebook of all calculations are included as Supplementary Material. Calculations were primarily performed on systems spanning a range of bulk H_2O (0.2–5.0 wt.%) and f_{O2} values ($0.0 < \Delta FMQ < +2.5$) but with constant bulk CO_2 and S (both 1000 μg/g). The bulk volatile contents are defined using total H_2O (all H dissolved in the melt reported as the equivalent amounts of H_2O), CO_2 (all C dissolved in the melt reported as the equivalent amount of CO_2), and S (all S dissolved in the melt reported as the equivalent amount of total S). Note that melt volatile contents are referred to using simply H_2O, CO_2, and S throughout, which accounts for the other volatile species present in the melt (e.g., H_2, CO, CH_4, H_2S). The initial f_{O2} value for a particular calculation is given by ΔFMQ_0, the difference in f_{O2} between the FMQ buffer at P^v_{sat} for the T of the calculation, where P^v_{sat} is the P of vapor-saturation for the melt composition of interest given its volatile concentrations (Hughes et al., 2024; Hughes, Saper, et al., 2023).

The behaviour of sulfur during degassing with varying initial water content

Solid curves in Figure 1 show *VolFe*-calculated, closed-system degassing paths from P^v_{sat} to 0.1 MPa for melts initially containing 1000 μg/g bulk CO_2 + 1000 μg/g bulk S at $\Delta FMQ_0=0$ with a bulk H_2O range from 0.2 to 5.0 wt.%. The P that degassing begins upon decompression (i.e., P^v_{sat}) increases with increasing bulk H_2O because the sum of the partial pressures of all vapor species must add up to the total P (e.g., Dalton, 1802; Hughes et al., 2024a; Verhoogen J, 1949). All volatiles begin degassing at P^v_{sat}: i.e., all volatiles will be present in the saturating vapor for $P \leq P^v_{sat}$, albeit in potentially small quantities (e.g., Métrich et al., 2009; Métrich & Wallace, 2009; Verhoogen J, 1949; Wallace et al., 2015). To compare changes in the P of degassing of different volatiles across different initial

conditions, we compare the P at which 10% of each volatile has degassed (i.e., the dissolved melt content of a particular volatile i is 10% its initial, undegassed value), which we term $P^{i}_{10\%}$ (i.e., filled circles in Figure 1).

Regardless of the bulk H_2O and S, CO_2 is always the first volatile to degas significantly in Figure 1 (i.e., $P^{CO_2}_{10\%} > P^{H_2O}_{10\%}$ and $P^{S_T}_{10\%}$: compare the P of the filled circles on the solid curves) because CO_2 is the most insoluble of these species (e.g., Dixon et al., 1995a). For 0.2 and 1.0 wt.% bulk H_2O, CO_2 degasses roughly linearly with decreasing P from P^{v}_{sat} to 0.1 MPa (i.e., melt CO_2 decreases roughly linearly with decreasing P along the red and purple solid curves in Figure 1b). For 3.0 and 5.0 wt.% bulk H_2O, CO_2 degassing also begins roughly linearly with a similar slope to the 0.2 and 1.0 wt.% bulk H_2O cases, which is similar to the results on MORB for 0–2 wt.% H_2O and 500 μg/g CO_2 in Dixon & Stolper (1995). However, the trend is offset to higher P's by approximately the P^{v}_{sat} for melts containing 3 and 5 wt.% bulk H_2O only (i.e., systems in which bulk CO_2 and S are 0 μg/g). At ≳95% degassing of the bulk CO_2, the rate of CO_2 degassing with respect to P decreases dramatically (i.e., solid curves in Figure 1b curve upward dramatically at lower P).

Degassing of H_2O has a strongly concave-down shape for all bulk H_2O values (Figure 1a). Significant degassing of H_2O occurs at a similar P to a melt containing only H_2O of the same bulk concentration would begin degassing (Dixon & Stolper, 1995): i.e., $P^{H_2O}_{10\%}$ (circle) and P^{v}_{sat} for the equivalent pure-H_2O system (grey curve) are very similar in Figure 1a. This significant degassing of H_2O also occurs at a similar P to the decreasing rate of CO_2 degassing with respect to P (Figure 1a and b). Additionally, there is a long, near-vertical tail at $P > P^{H_2O}_{10\%}$ corresponding to low degassing rates with respect to P whilst most of the CO_2 degasses (Figure 1a).

This behaviour of H_2O-CO_2 degassing is due to the dilution effect, as described in the Introduction (e.g., Anderson et al., 2024, 2025; Dixon & Stolper, 1995; Iacovino et al., 2021;

Lowenstern, 2001). Dilution by H_2O has a large effect on CO_2 degassing, causing CO_2 degassing at higher P than if it were the only volatile in the system. For instance, CO_2 degasses at increasingly higher P with increasing initial H_2O (i.e., $P_{10\%}^{CO_2}$ is a strong function of bulk H_2O, Figure 1b; e.g., Dixon & Stolper, 1995; Yip et al., 2022). This results from: (1) the high concentration of H_2O relative to CO_2 in the system, and (2) the low solubility of CO_2 relative to H_2O in most magmatic melts (e.g., Dixon et al., 1995a; Dixon & Stolper, 1995). This combination means the CO_2 degassing path is essentially just offset to higher P by roughly the solubility of pure-H_2O. The complementary dilution effect of CO_2 on H_2O degassing is more subtle (i.e., $P_{10\%}^{H_2O}$ is similar to P^v_{sat} for pure-H_2O; e.g., Dixon & Stolper, 1995) due to the low concentration of CO_2. However, the presence of CO_2 does result in a long tail of deep degassing of H_2O (from P^v_{sat} to ~$P_{10\%}^{H_2O}$; Figure 1a) due to CO_2 being highly insoluble. At higher initial CO_2 concentrations (e.g., > 1 wt.%), a more substantial effect on H_2O degassing occurs (e.g., Anderson et al., 2024, 2025; Dixon & Stolper, 1995), highlighting the importance of initial concentration on the effects of dilution (Figure S4a).

As for H_2O, the rate of S degassing with respect to P is small initially, leading to the deep, near-vertical tails at ~1000 μg/g S (Figure 1c). The rate of S degassing increases at a similar (although slightly higher) P relative to that at which the rate of H_2O degassing with respect to decreasing P increases dramatically, leading to strong downward curvatures of the degassing curves. By design, these 10% degassing P's for H_2O and S are all close to the position on their respective degassing curves at which the rate of degassing increases rapidly (i.e., 10% was chosen for this effect, compare the positions of the coloured circles in Figure 1a and c). It is interesting that $P_{10\%}^{H_2O}$ and $P_{10\%}^{S}$ are similar to each other for bulk H_2O's ranging from 0.2 to 5.0 wt.% (compare the positions of the circles of the same color in Figure 1a and c). Although there are subtle differences, deeper degassing of S also occurs when degassing is open- rather than closed-system (solid vs. dotted curves in Figure 1c).

Additionally, increasing the initial CO_2 content also increases $P_{10\%}^{S}$ (Figure S4c; e.g., Yip et al., 2022).

A key feature of Figure 1 is the increase in $P_{10\%}$ for *all* volatiles with increasing bulk H_2O of the melt at constant bulk CO_2 and S. For H_2O itself, the higher the melt H_2O, the greater the depth at which H_2O significantly degases. In the case that H_2O is the only volatile in the system, the P that H_2O begins to degas is simply the P on the solubility curve for pure-H_2O corresponding to the melt H_2O content (Figure 1a, e.g., Dixon & Stolper, 1995). The deepening of $P_{10\%}^{S}$ with increasing bulk H_2O is particularly dramatic (Figure 1c): the same melt with only 1000 μg/g S at ΔFMQ_0=0 would begin degassing at just ~0.5 MPa (Hughes, Saper, et al., 2023). The deepening of S degassing with increasing bulk H_2O is in overall agreement with the independent modelling of Ding et al. (2023) and Yip et al. (2022). We regard this as important validation of *Sulfur_X* (Ding et al., 2023) and *VolFe* given that they were developed independently and with different thermodynamic formulations, computational approaches, and approximations (see Figure S1 for a direct comparison of the results of *VolFe* and *Sulfur_X* output – *EVo* (Liggins, 2023; Liggins et al., 2020, 2022), that was used in Yip et al., 2022, uses a similar modelling approach to *VolFe*).

The behaviour of sulfur during degassing with varying initial oxygen fugacity

The speciation of H, C, and S both in silicate melt and vapor vary with f_{O2} and this results in variability of degassing paths when calculated over a sufficiently large range in ΔFMQ_0 (e.g., Gaillard et al., 2022; Holloway & Blank, 1994; Lo et al., 2021). Some of these effects are illustrated in Figure 2 by repeating the closed-system calculations from Figure 1 at a single bulk H_2O (3 wt.% H_2O + 1000 μg/g CO_2 + 1000 μg/g S) over the range of ΔFMQ_0 from 0.0 to +2.5, which spans abundant terrestrial magmas (e.g., Cottrell et al., 2021). For

$\Delta FMQ_0 > 0$, the H_2O and CO_2 degassing curves are essentially independent of ΔFMQ_0 (Figure 2a and b) because H_2O and CO_2 are calculated as the dominant H- and C-bearing vapor species and H_2O_T and $CO_{2,T}$ the dominant melt species (i.e., oxidised H- and C-bearing species in the melt: OH^- and H_2O_{mol} or $CO_{2,mol}$ and CO_3^{2-}, respectively; e.g., Armstrong et al., 2015; Hirschmann et al., 2012; Hughes et al., 2024a). In contrast, the speciation of S in vapor and melt vary significantly over this f_{O2} range (Figure 2f–h), resulting in observable variations in S degassing behaviour (Figure 2d and e).

The variation in ΔFMQ_0 causes systematic changes in the speciation of S in the melt and vapor at P^v_{sat} that can be understood by the chemical equilibria involving S-bearing species (e.g., Hughes et al., 2024a). For instance, the melt S^{6+}/S_T at P^v_{sat} varies from ~0 at ΔFMQ_0=0 (i.e., dissolved S in the melt is almost entirely sulfide: note that "sulfide" in this statement includes both H_2S and "other" S^{2-} species – e.g., FeS, MgS, etc. – collectively referred to as "$*S^{2-}$"; defined in Hughes et al., 2024a) to ~1 at ΔFMQ_0=+2.5 (i.e., almost entirely sulfate; Figure 2f). This is due to the sigmoidal relationship between S speciation in melt and f_{O2} (see eq. 20 in Hughes et al., 2024a – a factor of (M_S/M_{H2S}), the molecular weights of S and H_2S, is missing from the first term in the denominator: e.g., Baker & Moretti, 2011; Baumgartner et al., 2017; Fincham & Richardson, 1954; Gaillard et al., 2011, 2013, 2015; Gaillard & Scaillet, 2009; Hughes, Saper, et al., 2023; Moretti, 2021; Moretti & Ottonello, 2003, 2005). This change in S speciation in the melt from dissolved sulfide to sulfate causes a maximum in P^v_{sat} (i.e., the maximum in the curve defined by the stars in Figure 2c) due to the SS^{min} (Hughes et al., 2024; Hughes, Saper, et al., 2023). At constant P, T, and melt composition, the SS^{min} occurs at $S^{6+}/S_T \approx 0.75$ because when the vapor is SO_2-dominated the solubility of S^{2-} in the melt decreases with increasing f_{O2}, whilst the solubility of S^{6+} in the melt increases with increasing f_{O2} (e.g., Baker & Moretti, 2011; Cicconi et al., 2020; Ding et al., 2023; Fincham & Richardson, 1954; Hughes et al., 2023; Moretti et al., 2003; Moretti & Ottonello, 2005;

Papale et al., 2022). The SS^{min} occurs at *exactly* $S^{6+}/S_T = 0.75$ in the S-O system (i.e., no H and C) when the vapor consists of purely ideal SO_2 (i.e., no S_2; Hughes et al., 2023). The non-ideality of the vapor, presence of other vapor species (e.g., H_2O, CO_2, H_2S, etc.), presence of other S-bearing melt species (e.g., H_2S), and variations in fH_2O mean the SS^{min} occurs at $S^{6+}/S_T \approx 0.75$ in the C-H-S-O system (Hughes et al., 2024). The solubility of S^{2-} does not vary significantly when the vapor is dominated by H_2S but the transition from H_2S to SO_2 in the vapor happens at lower f_{O2} than the SS^{min} (e.g., Ding et al., 2023; Hughes et al., 2024a). Additionally, the proportion of S dissolved as H_2S in the melt (S_{H2S}/S_T) at P^v_{sat} decreases with increasing ΔFMQ_0 (Figure 2g). The relative proportions of dissolved H_2S to $*S^{2-}$ is essentially unchanging at P^v_{sat} because melt H_2O is constant such that f_{H2O} is essentially not varying (see eq. 19 in Hughes et al., 2024a). However, as melt S^{6+}/S_T increases with increasing ΔFMQ_0, $(*S^{2-} + S_{H2S})/S_T$ is decreasing such that S_{H2S}/S_T also decreases. The calculated equilibrium vapor composition also varies significantly with increasing ΔFMQ_0, with increasing proportions of SO_2 relative to H_2S at P^v_{sat} (Figure 2h).

From any given ΔFMQ_0, the *VolFe*-calculated f_{O2}-value varies with progressive depressurization and degassing (Figure 2c). Although H_2O and CO_2 degassing can cause changes in f_{O2} (e.g., Burgisser & Scaillet, 2007; Candela, 1986; Carmichael & Ghiorso, 1986; Gaillard et al., 2015; Gaillard & Scaillet, 2014; Herd & Benaroya, 2025; Mathez, 1984), for the f_{O2} range considered here the predominant effect is due to S degassing. Sulfur degassing leads to overall reduction for melts at lower f_{O2} where dissolved sulfide (S^{2-}) degasses to SO_2 (S^{4+}) because there is a +6 change in the redox state of S (red curves in Figure 2c; e.g. A. T. J. Anderson & Wright, 1972; Brounce et al., 2017; Burgisser & Scaillet, 2007; Cottrell & Kelley, 2011; de Moor et al., 2013; Gaillard et al., 2011, 2015; Hughes, Saper, et al., 2023; Métrich et al., 2009; Moussallam et al., 2014, 2016; O'Neill & Mavrogenes, 2022). Degassing of dissolved sulfide (S^{2-}) to H_2S (S^{2-}) is neutral in its effect on f_{O2} (e.g., de Moor et

284 al., 2013; Ding et al., 2023). Overall oxidation occurs due to S degassing at higher f_{O2} where
285 dissolved sulfate (S^{6+}) degasses to SO_2 (S^{4+}) due to the -2 change in the redox state of S (blue
286 curves in Figure 2c; e.g., Boulliung & Wood, 2022, 2023; de Moor et al., 2013; Farsang &
287 Zajacz, 2024; Gaillard et al., 2015; Hughes, Saper, et al., 2023; Métrich et al., 2009; O'Neill
288 & Mavrogenes, 2022). The boundary separating S-degassing induced reduction and oxidation
289 is the f_{O2} of the SS^{min} (de Moor et al., 2013; Hughes et al., 2024; O'Neill & Mavrogenes,
290 2022).

291 These f_{O2} variations as degassing proceeds lead to systematic changes in the S speciation
292 of the melt and vapor (Figure 2f–h) due to the same chemical equilibria described for the
293 changes at P^{v}_{sat} earlier in this section. However, H_2O begins degassing significantly at ~100
294 MPa (Figure 2a) causing f_{H2O} to decrease significantly from this P. This H_2O degassing at $P <$
295 100 MPa has a minor effect on the melt S^{6+}/S_T (see eq. 20 in Hughes et al., 2024a) but causes
296 S_{H2S}/S_T to decrease significantly (Figure 2g; see eq. 19 in Hughes et al., 2024a) and the
297 proportion of SO_2 to rapidly increase such that it is the dominant gaseous species for all f_{O2}
298 near the surface (Figure 2h: e.g., Ding et al., 2023; Farsang & Zajacz, 2024; further
299 explanation in Supplementary Material Section 2.2).

300 Based on our modelling, the extent of S degassing at any given value of $P \leq P^{v}_{sat}$ and
301 $P^{S}_{10\%}$ increases with increasing ΔFMQ_0 from 0 to +1.4 when the melt is sulfide-dominated
302 (i.e., see the downward pointing arrow in Figure 2c – note that ΔFMQ_0=+1.4 is close to the
303 SS^{min}; e.g., Ding et al., 2023; Gaillard & Scaillet, 2009; Hughes, Saper, et al., 2023). The
304 extent of S degassing then decreases as ΔFMQ_0 increases further to +2.5 when the melt is
305 sulfate-dominated (see the upward pointing arrow in Figure 2e; e.g., Boulliung & Wood,
306 2022, 2023; Hughes, Saper, et al., 2023; Yip et al., 2022). The predicted deeper S degassing
307 from a melt that begins degassing at an f_{O2} near the SS^{min} relative to the depths of degassing
308 of the same melt at higher and lower values of f_{O2} reflects the lower total S solubility at the

309 SS^{min} relative to melts at higher and lower f_{O2} (Backnaes & Deubener, 2011; Baker &
310 Moretti, 2011; Carroll & Rutherford, 1985; Cicconi et al., 2020; Ding et al., 2023; Fincham
311 & Richardson, 1954; Hughes et al., 2024; Hughes, Saper, et al., 2023; Katsura & Nagashima,
312 1974; Lesne et al., 2015; Matjuschkin et al., 2016; Moretti et al., 2003; Moretti & Ottonello,
313 2005; Nash et al., 2019; O'Neill & Mavrogenes, 2022; Papale et al., 2022). All other things
314 being equal (e.g., f_{O2}; bulk H_2O, CO_2, and S in Figure 2), $P_{10\%}^{S}$ increases (and thus S has
315 degassed more at any given $P \leq P^{v}_{sat}$) if the total S solubility is lower (as it is at the SS^{min};
316 Figure 2c). Hence, f_{O2}-dependent S speciation in the melt and vapor affects S degassing
317 through its effects on total S solubility as a function of f_{O2}.
318 The predominance of H_2S in the melt and vapor (Figure 2g and h) under relatively
319 reducing conditions (e.g., ΔFMQ_0=0) could suggest that it plays an important role in the
320 deeper degassing of S with increasing bulk H_2O. Ding et al. (2023), whilst not including an
321 explicit H_2S species in the melt, attributed the deeper degassing of S to a lowering of S
322 solubility by reaction of H_2O in the vapor with anhydrous sulfide species in the melt (e.g.,
323 FeS) to generate H_2S molecules which exsolve into the vapor and a direct effect of dissolved
324 H_2O on this partition coefficient. However, we observe deeper degassing of S in hydrous
325 melts when H_2S is artificially forced to be completely insoluble in the melt (i.e., H_2S is
326 present in the coexisting vapor but not in the melt) *or* if it is assumed to be completely absent
327 from the system (i.e., no H_2S is allowed to stabilize in either the melt or vapor; see
328 Supplementary Material Section 2.3 for more details on both of these numerical
329 experiments). Additionally, under oxidising conditions (i.e., $\Delta FMQ_0 > +1.4$): (1) H_2S is a
330 minor species in the melt (Figure 2g) and vapor (Figure 2h) for the parameters used in these
331 calculations (Table S2); and (2) *VolFe* does not currently include melt or vapor species that
332 contain both H^+ and S^{6+} (e.g., H_2SO_4). Similarly, there is no H_2O compositional term in the
333 sulfate capacity expression used in these calculations beyond a dilution of the concentration

of all oxides in the melt (O'Neill & Mavrogenes, 2022) that could indirectly lead to a connection between the solubilities of H_2O and S^{6+} in silicate melt (e.g., Moretti & Ottonello, 2005; although it has been suggested that inclusion of such an H_2O-affect could cause either deeper or shallower S degassing; Boulliung & Wood, 2022). Nevertheless, based on *VolFe*, deeper degassing of S from H_2O-rich magmas is still present under oxidizing conditions at a comparable magnitude to the reduced case (Figure 2c–e). That this effect is present in the (near) absence of H_2S in the system under oxidizing conditions suggests that H_2S does not play a definitive role in the *VolFe*-modelled effects of dissolved H_2O on the deepening of S degassing from basaltic magmas.

These observations demonstrate that in the context of *VolFe*: neither: (1) the presence or absence of H_2S species in the melt and/or vapor; nor (2) a direct influence of H_2O on S solubility (e.g., H_2SO_4 species in the melt or vapor; or a H_2O compositional term in the sulfide or sulfate capacity); nor (3) the transition from sulfide to sulfate as the dominant dissolved melt species with increasing f_{O2}, are likely to be the main drivers of the deeper degassing of S during ascent of hydrous magmas. These factors are predicted by *VolFe* to have effects on the details of S degassing, such as deepening S degassing for melts that begin degassing in the vicinity of the SS^{min} and minor changes in the P of degassing depending on whether H_2S is a melt and/or vapor species. However, our modelling suggests that something else must be responsible for the first-order result that, for a given anhydrous major element base composition, melts with higher bulk H_2O degas S at higher P than melts with less dissolved H_2O. As we anticipated in the Introduction and describe in detail in the following sections, we conclude that a "dilution effect" – driven mostly by the presence of H_2O – is primarily responsible for deeper degassing of S from natural, hydrous melts.

The behaviour of an inert, ideal volatile species during degassing

As illustrated in the previous section, the interactions between homogeneous and heterogeneous equilibria involving melt and vapor in S±H±C–bearing magmas are complex. As a consequence, the details of degassing behaviour can be hard to anticipate fully without an internally consistent thermodynamic model that incorporates the large number of potentially relevant independent interspecies interactions. In this section we consider the degassing behaviour of a fictive volatile component – referred to as "χ" – that does not have these complications (χ is referred to as "X" in Hughes et al., 2025, but to avoid confusion with mole fraction, etc., we use χ here). By definition, χ is an ideal volatile component that: (1) is present in the same form in melt and vapor; (2) does not react with other species in melt or vapor to form additional species; and (3) has a solubility function in melt unaffected by variations in f_{O2} or H_2O. As a tangible example, the noble gases would closely approximate the χ component (e.g., Carroll & Stolper, 1993; Iacono-Marziano et al., 2010). In the following calculations, the molecular weight of χ is chosen as 40 (i.e., it can be viewed as similar to Ar). We compare the *VolFe*-calculated degassing behaviour of such a component to that of S – especially the degree to which such a model component displays an increase in the *P* of significant degassing with increasing H_2O content of the system.

We define the equilibrium constant for χ (K_χ) as:

$$K_\chi = \frac{w_\chi^m}{p_\chi}, \quad (1)$$

where w_χ^m is the concentration of χ in the melt (μg/g) and p_χ is the partial pressure of χ in the vapor (MPa). For simplicity we choose K_χ to be independent of all other parameters, including *P*, *T*, and the concentrations of all other species in the melt and vapor (especially H_2O and CO_2). We initially choose a value of 450 μg/g/MPa for K_χ so that it mimics the

behaviour of S for the calculation with bulk concentrations of 3 wt.% H_2O + 1000 μg/g CO_2 at ΔFMQ_0=0.

In Figure 3 we show the effects of replacing S, with its full complexity resulting from the presences of multiple S-bearing species in melt and vapor; by χ, with its single species in both the melt and vapor and its strictly Henrian solubility function. The degassing curves in black for S and χ in Figure 3c are nearly identical, which is to some degree by design; i.e., the value of 450 μg/g/MPa for K_χ was chosen for this purpose. However, the excellent agreement between the *shapes* of these two degassing curves is not by design. The details of the shapes of the two black degassing curves in Figure 3c reflect the thermodynamic functions and interactions built into *VolFe*: i.e., the complex speciation in the melt and vapor of S, and in contrast, the simple, Henrian behaviour of the non-reacting χ species. The strong similarity of the shapes of the S and χ degassing curves suggests that the degassing behavior of S in these calculations is not strongly dependent on the details of S speciation in the melt or vapor, but instead depends primarily on the overall solubility of S in the melt, which is very similar to that of χ in Figure 3c. Moreover, changing bulk H_2O up to 5 wt.% or down to 1 wt.% deepens or shallows the degassing curves similarly for χ and S – again, with no adjustable parameters (i.e., K_χ = 450 μg/g/MPa for all three dashed curves in Figure 3c). Although the shapes of the S and χ curves for the 1 and 5 wt.% bulk H_2O curves are still similar, they are no longer essentially identical as they are for the 3 wt.% bulk H_2O curves. The progressive overall deepening of S and χ degassing with increasing bulk H_2O are very similar (i.e., $P^{S}_{10\%}$ and $P^{\chi}_{10\%}$ are similar). The solid and dashed degassing curves for H_2O (Figure 3a) and CO_2 (Figure 3b) are essentially indistinguishable, reflecting the similarity in the behaviour of S and χ.

Figure 4a shows how tuning K_χ (vertical dashed lines in Figure 4b) can enable the degassing behaviour of χ to mimic the behaviour of S when ΔFMQ_0 is varied. In contrast to χ,

405 the “solubility” of S in the melt along its degassing curve is not constant (Figure 4b),
406 reflecting the fully complex thermodynamic characterization of heterogeneous and
407 homogeneous equilibria among all S-bearing species in melt and vapor used by *VolFe*.
408 Although the K_χ values are constant (by assumption) and the calculated K_S values are not
409 (Figure 4b), the behavior of χ and S are still essentially indistinguishable (Figure 4a). These
410 comparisons of the degassing curves of S and χ demonstrate that an inert χ component
411 mimics the degassing of S if it assigned a similar solubility to total S (Figure 3 and Figure 4).
412 The major element melt composition can strongly influence S solubility through the
413 compositional dependencies of the sulfide and sulfate capacities (e.g., Boulliung & Wood,
414 2022, 2023; Moretti & Ottonello, 2005; O’Neill, 2021a; O’Neill & Mavrogenes, 2002,
415 2022a). Although we anticipate that the χ degassing curves will mimic the S degassing curves
416 for other melt compositions as well, the equilibrium constant of χ used in the model would
417 also have to vary with melt composition in proportion to the variations in total S solubility.
418 In summary, increasing the bulk melt H_2O content causes deeper degassing (i.e.,
419 increases $P_{10\%}$) even for an ideal and inert volatile component with only a single vapor
420 species and melt species (Figure 3). This replicates the dependence of S degassing with
421 variable bulk H_2O and initial f_{O2} despite the absence of the complexity of melt and vapor
422 speciation characteristics of S. This suggests that such complexities do not play significant
423 roles in the variability in the depth of significant degassing S in magmas spanning ranges of
424 bulk H_2O and initial f_{O2}. In the next section, we describe how the so-called “dilution effect”
425 (e.g., O. E. Anderson et al., 2024, 2025; Dixon & Stolper, 1995; Gonnermann &
426 Mukhopadhyay, 2007; Iacovino et al., 2021; Lowenstern, 2001; Webster & Botcharnikov,
427 2011) can provide a straightforward explanation of the similar behavior of S and χ during
428 degassing and guidance into the expected degassing behavior of systems in which multiple

volatile components are actively and simultaneously degassing from melts on ascent of magmas.

Dilution-driven degassing

It has long been known that the solubility of S in silicate melts is a strong function of f_{O2}, as f_{O2} affects the S^{6+}/S^{2-} ratio of the melt (Carroll & Rutherford, 1985; Fincham & Richardson, 1954; Wallace & Carmichael, 1994) and the SO_2/H_2S ratio of the vapor (e.g., Symonds et al., 1994; Whitney, 1984). These changes in melt S^{6+}/S^{2-} and vapor SO_2/H_2S result in shifts in the dominant heterogeneous equilibria that control the total S contents of vapor-saturated melts (e.g., Fincham & Richardson, 1954; Hughes, Saper, et al., 2023; Moretti & Ottonello, 2003). It may thus appear at first somewhat surprising that the behaviour of the fictive volatile species χ – which does not have multiple molecular or heterovalent species and is assumed by definition to have no chemical interactions with water in the melt or vapor – reproduces so well the effects of H_2O and f_{O2} on the degassing curves of S when χ is assigned a partitioning between vapor and melt similar to that of the total S under similar conditions (Figure 3 andFigure **4**). In this section, we describe how this behaviour predicted by *VolFe* – and in particular the deepening of χ degassing from the melt as the H_2O content of the melt increases and the degree to which it matches the details of S deassing – can be relatively simply understood with reference to the phenomenon of "dilution" (e.g., O. E. Anderson et al., 2024, 2025; Dixon & Stolper, 1995; Gonnermann & Mukhopadhyay, 2007; Iacovino et al., 2021; Lowenstern, 2001; Webster & Botcharnikov, 2011).

Dilution-driven degassing by isobaric addition of an insoluble volatile species to the vapor

Suppose we start with a silicate melt and a multicomponent vapor in equilibrium at constant P and T. For this simple example, we assume that the vapor is an ideal gas and that each of the i volatile species dissolved in the melt are ideal species (i.e., eq. 1 applies for all of the i species). Starting from this equilibrium state, suppose we instantaneously add a finite amount of an additional, perfectly insoluble component to the system at constant P and T. The new component will partition completely into vapor as it is insoluble but since P is constant, the p_i's of all other species in the vapor must decrease proportionately due to dilution with the newly introduced insoluble volatile component. However, the instantaneous decrease in the p_i for each of the i soluble species results in the melt and vapor being out of equilibrium: i.e., w_i^m/p_i has increased for each vapor species due to the instantaneous decrease in p_i but the unchanged value of w_i^m for each melt species. As a result, this initial value of w_i^m is higher than the equilibrium value given the new, lower value of p_i. In other words, the addition of the new component to the vapor means the melt is now oversaturated with respect to all the initial components in the vapor. In response, some of each of the i soluble volatile component must transfer from the melt to the vapor (i.e., degas), decreasing w_i^m and increasing p_i until the equilibrium value of K_i is re-achieved. The p_i of the instantaneously added completely insoluble component will decrease due to dilution resulting from the transfer of dissolved volatiles from the melt to the vapor, resulting in further adjustment of the concentrations of these components in the melt and vapor. Eventually the system will reach a new equilibrium state that is degassed in all volatiles relative to the initial state, despite the fact that the equilibrium constant (i.e., the value of K_i) for each species has not changed.

A simplified illustration of this process is shown in Figure 5 for a system with two ideal volatile components: "Y" is soluble in the melt (i.e., $K_{\text{"Y"}} > 0$ μg/g/MPa) whilst "Z" is

insoluble (i.e., $K_{"Z"} = 0$ μg/g/MPa; note that this cannot be the case in real systems). Initially, there is 10 μg/g "Y" dissolved in the melt co-existing with a pure-"Y" vapor at 100 MPa and 1200 °C (Figure 5a). At constant *P* and *T*, "Z" is added to the system such that the vapor is 50:50 mol.% "Y" and "Z", causing the volume of vapor to increase because the number of moles of gas species in the vapor increases (Figure 5b). To achieve equilibrium given that $K_{"Y"}$ remains constant, "Y" degasses leaving only 5 μg/g "Y" in the melt (Figure 5b). This particular process could apply to pure-CO_2 gas streaming through a column of water-bearing magma at low *P* where CO_2 is not very soluble; such a process would progressively remove H_2O from the melt, and it could eventually nearly entirely dehydrate the magma (e.g., A. T. J. Anderson et al., 1989).

The central role of dilution by water degassing in the deepening of sulfur degassing

In contrast to the simple example of the effects of dilution illustrated in Figure 5 and described in the previous section, for closed-system degassing, the composition of the system is held constant. Hence, dilution of volatile components in the vapor by addition of a new volatile component to the system (or more of a volatile that is already present) and the resultant degassing of other volatile components in the melt as described in the previous section do not apply in detail to a closed-system (nor is addition of a *completely* insoluble volatile component as previously described realistic). However, decompression-driven degassing of more volatile components and/or of components present in the system at high concentrations relative to other volatile species (e.g., H_2O relative to all other volatile components as considered here) will have the same overall effect of diluting all other components in the vapor (i.e., increasing their $P_{10\%}$). This dilution in a closed-system drives "additional" degassing of all other species relative to what would occur if the other volatiles were not present in the undegassed melt (Dixon & Stolper, 1995). This has been used to

explain the behaviour of mixed H_2O-CO_2 degassing (e.g., O. E. Anderson et al., 2024, 2025; Dixon & Stolper, 1995; Iacovino et al., 2021; Lowenstern, 2001) and increased He degassing in CO_2-rich OIBs compared with MORBs (e.g., Gonnermann & Mukhopadhyay, 2007). In this section, by comparing *VolFe*-modeled degassing of S to that of the inert and ideal species χ, we conclude that the presence of H_2O is the principal driver of deep degassing of S during closed- and open-system degassing of hydrous magmas (Figure 3c; Dixon & Stolper, 1995) via the significant dilution of S in the vapor by the degassing of H_2O as the magma decompresses (Gaillard & Scaillet, 2009).

We can do a thought experiment using a simplified version of the calculations with bulk concentrations of 3 wt.% H_2O + 1000 μg/g CO_2 + 1000 μg/g χ at ΔFMQ_0=0 to explore the dilution effect during closed-system degassing (i.e., black dashed curves in Figure 3 are reproduced in Figure 6a–c). For these conditions, the melt becomes vapor saturated at 262.9 MPa (i.e., P^v_{sat} = black star) and there is no vapor (Figure 6d). After closed-system degassing to 260.0 MPa, the concentrations of H_2O and χ in the melt are essentially the same as at P^v_{sat} because of their high solubility, but the CO_2 content of the melt has decreased to 983 μg/g (Figure 6a–c and e). There is a small amount of coexisting vapor (0.002 wt.%, its volume relative to the melt is exaggerated in Figure 6e to be visible) with a composition of ~71 mol.% CO_2, ~28 mol.% H_2O, and ~1 mol.% χ (their relative molar proportions are shown by their relative area in the vapor in Figure 6e).

We now instantaneously bring the melt and vapor to 87.5 MPa, where 10% of χ would have degassed under equilibrium conditions. However, we prevent CO_2 and χ from degassing such that the concentration of CO_2 and χ in the melt and number of moles of CO_2 and χ in the vapor stay as they were at 260.0 MPa (Figure 6b, c, and f). Only H_2O is allowed to degas (i.e., its concentration in the melt decreases and the number of moles of H_2O in the vapor

526 increases), which we do in a simplified way by setting the H_2O content of the melt to that of
527 the equilibrium value for the true degassing calculation (i.e., 2.85 wt.%, the circle in Figure
528 6a) and calculating the number of moles of H_2O transferred to the vapor. This is like there
529 being a semi-permeable membrane present between the melt and vapor that lets H_2O degas,
530 but not CO_2 or χ. This results in a melt containing 2.85 wt.% H_2O, 983 μg/g CO_2, and ~1000
531 μg/g χ, with a vapor composition of nearly pure-H_2O and negligible CO_2 (0.005 mol.%) and χ
532 (0.00006 mol.%) (Figure 6a–c and f). Note that the system is technically vapor-
533 undersaturated because the sum of the p_i's does not equal the total P (H_2O would technically
534 degas more than in the true degassing calculation to compensate for the lack of CO_2 and χ
535 degassing) but for the purpose of this illustration, this is not important. The amount of CO_2
536 and χ in the vapor has been highly diluted by the degassed H_2O causing the melt and vapor to
537 be highly out of equilibrium for CO_2 and χ (Figure 6b, c, and f). For instance, the equilibrium
538 constant for χ should be 450 μg/g/MPa but the ratio of w_χ^m to p_χ is 195,980 μg/g/MPa!
539 Hence, for CO_2 and χ to achieve equilibrium between the melt and vapor they must degas,
540 lowering their melt-vapor ratios until it reaches their equilibrium constant (eq. 1, Figure 6e).
541 This highlights how dilution can occur without the external addition of a volatile, but instead
542 by degassing of a volatile already present in the system.

543 This analysis of how the transfer of an abundant volatile component during degassing
544 can drive enhanced transfer of other dissolved species from the melt to the vapor highlights
545 that the dilution effect can be quite dramatic. For instance, increasing the bulk H_2O from 0.2
546 to 5.0 wt.% with 1000 μg/g CO_2 + 1000 μg/g S at ΔFMQ_0=0 increases $P_{10\%}$ from 181.5 to
547 340.3 MPa for CO_2 and 3.7 to 199.3 MPa for S (Figure 1b and c). The effect of dilution by a
548 volatile (e.g., H_2O) on the degassing behaviour of another volatile (e.g., CO_2 and S) depends
549 on their equilibrium constants (eq. 1) and concentrations of the volatiles relative to one
550 another (Dixon & Stolper, 1995). All things being equal, for either: (1) a smaller equilibrium

551 constant, or (2) a higher concentration of a volatile, the deeper its $P_{10\%}$ and the larger its
552 dilution effect on other volatiles (see Supplementary Material Section 2.4 for more details).
553 At ΔFMQ_0=0, H_2O is the most soluble species, followed by S, and CO_2 is the most insoluble
554 (i.e., H_2O has the largest equilibrium constant, and CO_2 the smallest). Water has a large
555 dilution effect on S (and CO_2) in hydrous magmas because of the high concentration of H_2O
556 relative to S (and CO_2: 0.1 vs. up to 5 wt.%). If the equilibrium constant for S or its typical
557 concentration in melts were higher or lower, the impact of dilution by H_2O would be different
558 and S could even become a more important diluter (Figure S4, S5, and S6). The long-tail of
559 deep degassing of S (up to ~10% of S for the degassing curves in Figure 1c) is related to
560 dilution of S by CO_2, because S has a larger equilibrium constant compared to CO_2, even
561 though their bulk concentrations by weight prior to degassing are identical. Although H_2O is
562 an important diluter, CO_2 concentrations on the order of a weight percent (or higher) in some
563 basaltic parental magmas mean it can be an important diluter in certain situations (Figure S4;
564 e.g., O. E. Anderson et al., 2024, 2025). More generally, volatiles that have high equilibrium
565 constants (i.e., that are highly soluble in the melt, such as Cl; e.g., Thomas & Wood, 2022)
566 will be less affected by dilution than those that are relatively insoluble in the melt.

567 It should be emphasized that f_{O2} does affect the speciation of S in both the melt and
568 vapor. Thus, the analogy between the behavior of S and that of a simplified inert and ideal
569 "χ" component during H_2O-dominated dilution degassing has its limits. In particular, care
570 should be taken when comparing processes across large ranges of f_{O2}, over which S-
571 speciation in the melt and vapor can change significantly. For example, the solubility of total
572 S in basaltic melts has a minimum near the f_{O2} of the SS^{min}, and the presence of H_2S in the
573 melt and/or vapor and its effects on total S solubility are also f_{O2}-dependent (e.g., Figure 2).
574 However, as discussed previously, these effects are secondary in comparison to the effect of
575 dilution by H_2O on the effects of degassing of S from hydrous magmas. The dilution effect

we have described here is inherent to any degassing models during closed-system degassing that include mass balance between the melt and vapor and requires that the total P is the sum of all p_i's.

Further impacts of dilution-driven degassing of sulfur in natural magmas

It is beyond the scope of this paper to delve into all possible petrological and volcanological observations that could be related to the dilution effect of H_2O on S degassing. We comment here briefly on how this dilution effect may contribute to understanding differences in the behaviour of S during degassing for magmas in different tectonic settings and interpreting the C/S ratios of volcanic gases.

Extent of dilution-driven degassing of sulfur by water across tectonic settings

The bulk H_2O content of magmas varies markedly across different tectonic settings (e.g., Wallace et al., 2015). The S contents of submarine MORBs suggests that little if any S degassing occurs prior to them erupting on the sea floor (e.g., Moore & Fabbi, 1971; Wallace & Carmichael, 1992; Wallace & Edmonds, 2011), unless they reach shallow water depths (e.g., <200 m on the Reykjanes Ridge; e.g., Moore & Schilling, 1973). This is consistent with their low H_2O content (~0.2 wt.%, e.g., Wallace et al., 2015), which results in little dilution of S by H_2O degassing (e.g., red curve for 0.2 wt.% bulk H_2O in Figure 1c), leading to the conclusion that S degassing is at most a minor phenomenon for most submarine MORB magmas. Similarly, magmas at Kīlauea and Mauna Kea are thought to degas S at relatively shallow depths (e.g., Dixon et al., 1991; Gerlach & Thomas, 1986; Lerner et al., 2021; Moore & Clague, 1987; Moore & Fabbi, 1971; Moore & Schilling, 1973; Moore & Thomas, 1988; Moussallam et al., 2016; Wallace & Carmichael, 1992; Wallace & Edmonds, 2011), which is

599 consistent with their low H_2O content (~0.3–0.8 wt.%; e.g., Seaman et al., 2004), again
600 causing some – but relatively little – dilution. Water-poor magmas closer to the SS^{min} (e.g.,
601 Mauna Loa; Wieser et al., 2025) display deeper degassing due to the lower solubility of total
602 S.

603 In contrast, arc magmas are hydrous (average ~4 wt.% and potentially up to 7 wt.%; e.g.,
604 Plank et al., 2013; Wallace et al., 2015), which causes large amounts of dilution of S by H_2O
605 and deep degassing of S in these magmas (e.g., Figure 1c). This transfers S from the melt to
606 the vapor, which can be released deep from ascending basaltic magmas. If this vapor
607 decouples from the ascending magma (i.e., approximating open-system degassing), the vapor
608 can migrate to shallower, more evolved magmas, providing additional S which could then
609 contribute to the "excess sulfur problem" (e.g., Christopher et al., 2010; Di Muro et al., 2008;
610 Edmonds et al., 2010; Pallister et al., 1992; Roberge et al., 2009; Wallace, 2001). Similarly,
611 this S derived from deep degassing of basaltic magmas may contribute to triggering extensive
612 precipitation of sulfide ores in porphyry copper deposits (e.g., Blundy et al., 2015; Hattori &
613 Keith, 2001). These effects are amplified by these magmas often having an f_{O2} near the SS^{min},
614 decreasing the solubility of S and increasing even further the potential impact of deeply
615 degassed S on shallower magmas and eruptive processes (e.g., Ding et al., 2023; Hughes,
616 Saper, et al., 2023; Nilsson & Peach, 1993).

617 Influence of dilution-driven degassing of sulfur by water on vapor C/S ratios

618 Deep degassing of S from water-rich arc magmas would also influence the C/S ratio of
619 gases measured at volcanic vents, which is commonly used to monitor volcanoes because of
620 its link to the depth of vapor segregation from the magma (i.e., magma depth; Aiuppa et al.,
621 2007, 2017; Burton et al., 2007; de Moor et al., 2016; Ding et al., 2025; Giggenbach, 1996;
622 Iacovino, 2015; Kern et al., 2022). In volcanoes without significant hydrothermal systems,

623 CO_2-rich gases (i.e., high C/S ratios) are assumed to reflect gases separating from magmas
624 that are degassing deep because of the relatively low solubility of CO_2 compared to other
625 volatiles such as S (e.g., Aiuppa et al., 2007; Kern et al., 2022). Likewise, the high solubility
626 of S relative to CO_2 has typically been taken to mean a magma would need to reach relatively
627 low *P* before it would degas significant S and generate vapors with low C/S (e.g., Aiuppa et
628 al., 2007; Kern et al., 2022). Together, these expected variations lead to decreasing C/S ratios
629 as magmas degas during ascent (e.g., Aiuppa et al., 2007; Kern et al., 2022).

630 Figure 7 demonstrates that the large dilution effect of H_2O on S results in C/S ratios that
631 – at any given *P* during closed- or open-system degassing – are also highly dependent on the
632 bulk H_2O content of the magma. Lower C/S ratios at a given *P* are characteristic of the vapor
633 if the bulk H_2O content of the magma is higher, reflecting the more effective "driving" of S
634 from melt to vapor via dilution (Figure 7a). Therefore, knowledge of the initial H_2O content
635 of the melt (in addition to f_{O2}, that also has a significant control on the C/S ratio at a given
636 depth; Figure 2i) is required to estimate accurate depths of magmatic degassing from the C/S
637 ratio of the gas (although currently different degassing tools give very different results for the
638 same conditions, Figure S1, which must also be resolved: e.g., comparison of various
639 degassing tools in Ding et al., 2025; Hughes, Ding, et al., 2023; Hughes et al., 2025). For
640 example, a C/S ratio of 20 could be produced from a magma at 13.0 MPa with 0.2 wt.% bulk
641 H_2O or 260.0 MPa for 5 wt.% bulk H_2O, or ~260 to ~140 MPa with 3 wt.% H_2O depending
642 on ΔFMQ_0 (grey dashed vertical line in **Figure *2***i and Figure 7a). Therefore magmas may be
643 degassing S much deeper than initially assumed, potentially increasing the time between
644 observing low C/S ratios and eruption for water-rich volcanoes, although this is highly
645 dependent on ascent rate.

646 The model curves for 3 and 5 wt.% water are strongly concave up and nearly vertical at
647 $P <$ ~100 MPa and ~200 MPa, respectively (the approximate *P*'s at which substantial

degassing of H_2O and S begin to degas, Figure 1a and c; Figure 7). In contrast, for 0.2 and 1.0 wt.% H_2O, the degassing curves are concave down for most of this shallow *P* range (Figure 7b). As a result, the C/S ratio during shallow degassing of water-rich magmas is not expected to vary much during their final ascent, in contrast to relative water-poor magmas (Figure 7). Magmas often stall at the depth of substantial degassing of H_2O due to the increased magma viscosity triggered by dehydration-driven crystallisation and increased melt viscosity (e.g., Cashman & Blundy, 2000; Ding et al., 2025; Rasmussen et al., 2022). Thus, as a consequence of the effects of dilution by H_2O degassing on the degassing of S, our calculations suggest that shallow magma ascent after potential stalling for water-rich magmas maybe essentially "invisible" using the C/S ratio, potentially reducing its effectiveness at monitoring magma ascent prior to eruption (Figure 7).

Summary

In water-poor magmas, S usually begins to degas significantly at shallow levels based on observations of MORBs and OIBs; its known partitioning between melt and vapor; and its typically low concentrations in magmas (e.g., Dixon et al., 1991; Lerner et al., 2021; Moore & Clague, 1987; Moore & Fabbi, 1971; Moore & Schilling, 1973; Moore & Thomas, 1988; Moussallam et al., 2016; Wallace & Carmichael, 1992; Wallace & Edmonds, 2011; Wieser et al., 2025). However, hydrous magmas are thought to degas S at much greater depths based on observations from arc volcanoes, experiments, and numerical modelling of degassing (e.g., Boulliung & Wood, 2022; Brounce et al., 2016; Davis et al., 1991; Ding et al., 2023; Edmonds & Wallace, 2017; Nilsson & Peach, 1993; Rasmussen et al., 2020; Wallace & Edmonds, 2011; Yip et al., 2022). Moreover, at a given initial f_{O2} and amount of dissolved S, the magnitude of the deepening of significant degassing of S is strongly and positively

672 correlated with the amount of dissolved H_2O. The deep degassing of S from hydrous mafic
673 magmas is likely important in igneous petrology, volcanology, and ore genesis in that it
674 provides a mechanism for deep mobilization of S into the vapor phase (e.g., Blundy et al.,
675 2015; Christopher et al., 2010; Di Muro et al., 2008; Edmonds et al., 2010; Hattori & Keith,
676 2001; Pallister et al., 1992; Roberge et al., 2009; Wallace, 2001).

677 Explanations of this large effect of H_2O on the depth of S degassing have mostly
678 focussed on changes in the partitioning of S in the melt and vapor related to hydrous magmas,
679 which are also often oxidised hydrous (e.g., Ding et al., 2023; Métrich et al., 2009; Nilsson &
680 Peach, 1993; Wallace & Edmonds, 2011; Zajacz et al., 2012). However, the influence of the
681 degassing of other volatiles such as CO_2 and H_2O has also been suggested (Davis et al., 1991;
682 Dixon & Stolper, 1995; Wallace & Edmonds, 2011) and H_2O degassing dilutes S in the vapor
683 (Gaillard & Scaillet, 2009). We used the Python package *VolFe* to explore the effects of
684 varying the bulk H_2O content and f_{O2} of a basaltic melt on the degassing behavior of S. We
685 found that an inert and ideal volatile species also displayed deeper degassing with increasing
686 bulk H_2O, highlighting that the complex chemical interplays between H_2O and S are not the
687 main drivers of deep degassing. Instead, we propose that the deepening of S degassing that
688 correlates with increases in the bulk melt H_2O content is dominantly an example of the
689 "dilution" effect during degassing (e.g., O. E. Anderson et al., 2024, 2025; Dixon & Stolper,
690 1995; Gaillard & Scaillet, 2009; Gonnermann & Mukhopadhyay, 2007; Iacovino et al., 2021;
691 Lowenstern, 2001; Webster & Botcharnikov, 2011). In its simplest terms for this case,
692 transfer of H_2O from melt to vapor during decompression "dilutes" all other components in
693 the vapor (i.e., decreases their thermodynamic activity and fugacity in the vapor; Gaillard &
694 Scaillet, 2009). As a result, the vapor becomes undersaturated with respect to the melt in S,
695 C, and any other volatiles in the system, and melt-vapor equilibrium is only re-achieved by
696 transfer of S, C, etc. from the melt into the vapor (i.e., degassing), increasing their

activities/fugacities until the vapor and the melt are in equilibrium. The sulfur solubility minimum additionally deepens the degassing of S due to the lower total solubility of S (e.g., Ding et al., 2023; Hughes, Saper, et al., 2023; Nilsson & Peach, 1993).

Based on our numerical experiments, the details of the dilution process depend strongly on the equilibrium constant of the volatile component relative to that of H_2O and their relative concentrations (Dixon & Stolper, 1995). For systems with significantly different absolute and relative concentrations of H_2O, CO_2, and S; f_{O2}; major element melt composition; and additional volatile components (e.g., rare gases, Cl, etc.), *VolFe* and/or other software packages could be readily modified to anticipate the consequences of dilution in a broader petrological and volcanological context.

Data availability statement

The *VolFe* Python package is freely available on GitHub (https://github.com/eryhughes/VolFe) and has been archived in Zenodo (Hughes, Liggins, & Wieser, 2025). The Jupyter Notebook to execute the calculations using *VolFe* and reproduce the graphs in this paper, the input Python files to execute the calculations using *Sulfur_X*, as well as all model outputs presented in this study, are included as Supplementary Material.

Funding

This work was supported by the New Zealand Ministry of Business, Innovation and Employment (MBIE) through the Strategic Science Investment Fund – Hazards and Risk Management [contract C05X1702, supporting ECH].

Figures

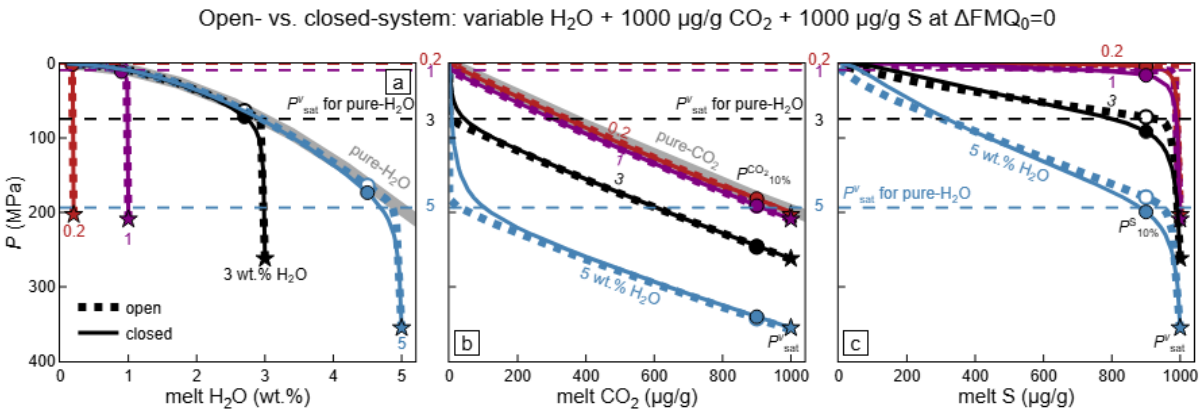

Figure 1. Effect of varying bulk H_2O on the melt volatile content during equilibrium, isothermal, decompression-induced, closed- and open-system degassing. The initial conditions are bulk concentrations of variable H_2O + 1000 µg/g CO_2 + 1000 µg/g S at ΔFMQ_0=0, where curve colour indicates bulk H_2O: 0.2 (red), 1.0 (purple), 3.0 (black), and 5.0 (blue) wt.% (labelled on each curve); and curve style indicates degassing style: closed (solid) and open (dotted). Concentration dissolved in the melt of **(a)** H_2O, **(b)** CO_2, and **(c)** S. Symbols indicate the location of P^v_{sat} (star) or $P^i_{10\%}$ (circle), which are labelled in (b) and (c). The closed-system degassing curves for pure H_2O and CO_2 are shown as a thick grey curves in (a) and (b), respectively (not shown in c: the same melt containing only 1000 µg/g S would begin degassing at ~0.5 MPa: Hughes, Saper, et al., 2023); and the thin, horizontal, dashed lines in all panels show the P where pure H_2O would begin to degas (i.e., P^v_{sat} for pure H_2O with the same bulk H_2O, labelled in between panels).

Alt text: Graphs showing the showing the concentration of water, carbon dioxide, and sulfur dissolved in the melt decreasing with decreasing pressure during open- and closed-system degassing for three different initial water concentrations of 0.2, 1, 3, and 5 weight percent. The depth at which ten percent of water and sulfur has degassed is similar to the depth at which ten percent water in the pure-water system would have degassed.

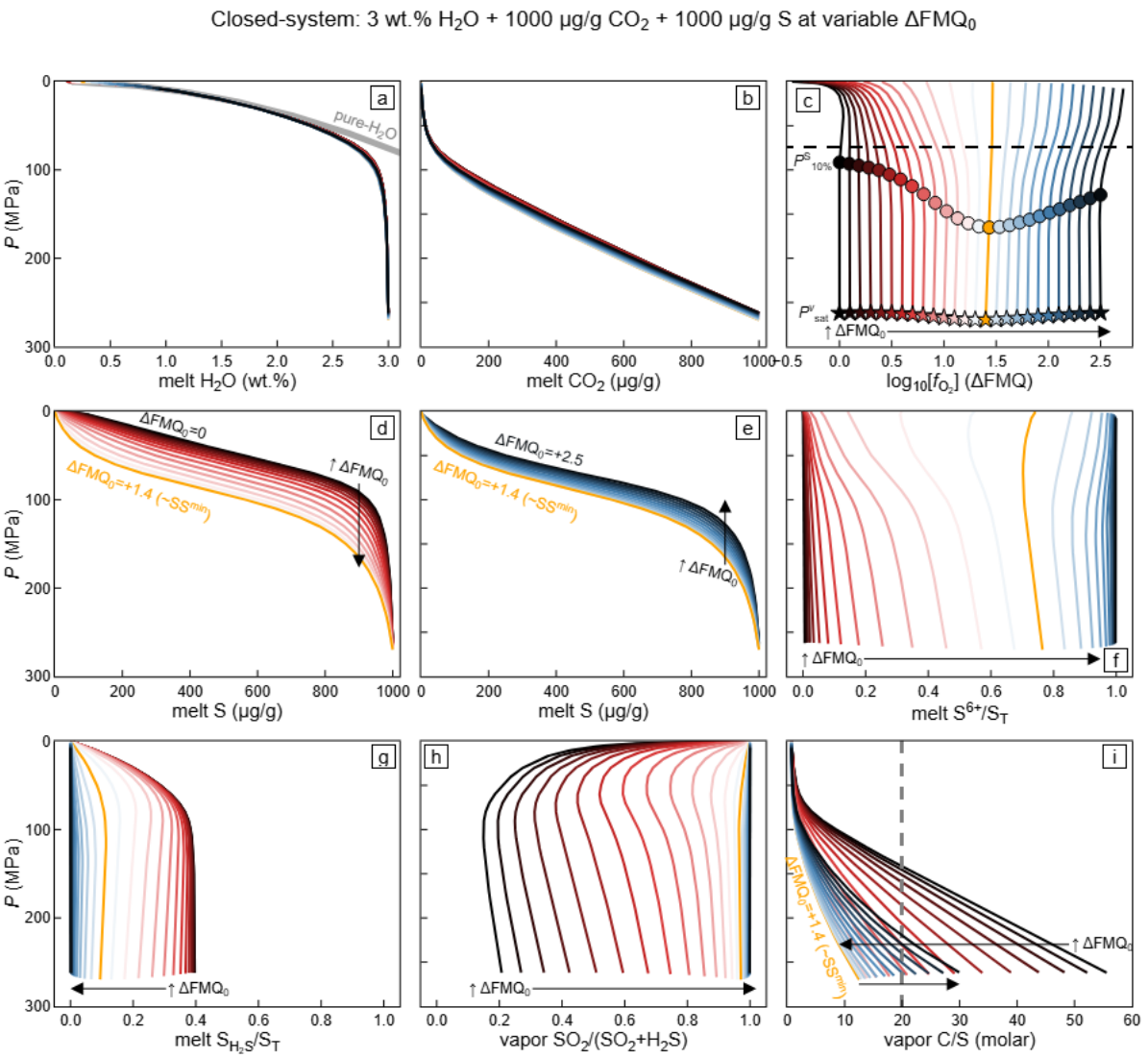

Figure 2. Effect of varying initial oxygen fugacity (ΔFMQ_0) on melt and vapor compositions during equilibrium, isothermal, decompression-induced, closed-system degassing. The initial conditions are bulk concentrations of 3 wt.% H_2O + 1000 µg/g CO_2 + 1000 µg/g S at $0 < \Delta FMQ_0 < +2.5$ in steps of 0.1, where curve colour indicates ΔFMQ_0: 0 (black, as in Figure 1), +0.1 to +1.3 (dark red through to light red), +1.4 (closest to SS^{min}, yellow), and +1.5 to +2.5 (light blue through to dark blue) (see panel (c) for exact colours). Concentration dissolved in the melt as a function of P of: **(a)** H_2O (including for pure H_2O as a thick grey curve: i.e., without C or S in the system); **(b)** CO_2; and **(d** and **e)** S – as the curves would overlap, (d) shows $0 < \Delta FMQ_0 < +1.4$ and (e) shows $+1.4 < \Delta FMQ_0 < +2.5$. Also as functions of P: **(c)** oxygen fugacity, where the high-P end of each curve corresponds to ΔFMQ_0 (i.e., at P^v_{sat}, stars)

and $P^{S}_{10\%}$ is shown by circles (corresponds to the black vertical arrows in d and e) – the horizontal black-dashed line shows for comparison the P^{v}_{sat} for a system with 3 wt.% pure H_2O (i.e., no C or S) would begin degassing; **(f)** S^{6+}/S_T in the melt; **(g)** the proportion of S dissolved as H_2S relative to total S (S_{H2S}/S_T) in the melt; **(h)** $SO_2/(SO_2+H_2S)$ and **(i)** C/S in mole fraction of the vapor coexisting with the partially degassed melt (where the vertical, dashed line indicates C/S = 20 in i). The direction of increasing ΔFMQ_0 in panels (c–f) is shown by a black, thin arrow and labelled.

Alt text: Graphs showing the melt and vapor compositions during degassing for a melt initially containing 3 weight percent water, 1000 micro-grams per gram carbon dioxide, and 1000 micro-grams per gram sulfur at initial oxygen fugacities ranging from 0 to plus 2.5 delta F M Q. All values are against pressure. Panel A shows water concentration in the melt. Panel B shows carbon dioxide concentration in the melt. Panel C shows oxygen fugacity. Panel D shows sulfur concentration in the melt for initial oxygen fugacities from 0 to plus 1.4 delta F M Q, which is at the sulfur solubility minimum, whilst plus 1.4 to plus 2.5 are shown in Panel E. Panel F shows the sulfur 6 plus over total sulfur ratio in the melt. Panel G shows the sulfur as hydrogen sulfide over total sulfur ratio in the melt. Panel H shows the sulfur dioxide over sulfur dioxide plus hydrogen sulfide ratio in the vapor. Panel I shows the carbon to sulfur ratio in the vapor.

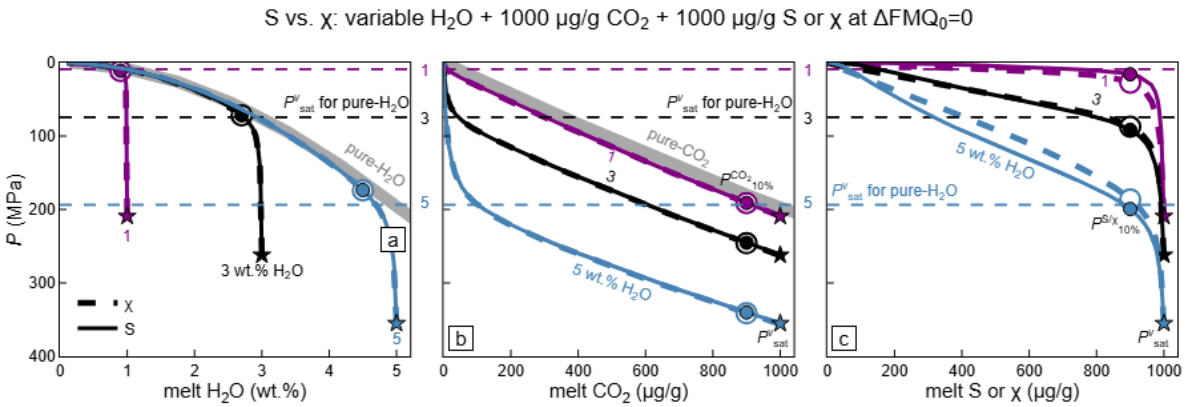

768

769 **Figure 3.** Comparison of the effect of including S or χ and varying bulk H_2O on the melt
770 volatile content during equilibrium, isothermal, decompression-induced, closed-system
771 degassing. The initial conditions are bulk concentrations of variable H_2O + 1000 µg/g CO_2 +
772 1000 µg/g S or χ at ΔFMQ_0=0. Concentration dissolved in the melt of **(a)** H_2O, **(b)** CO_2, and
773 **(c)** S or χ. Colour, style, and shapes of curves, lines and symbols as in Figure 1, with the
774 addition that dashed curves and open symbols indicate the presence of χ (solid curves and filled
775 systems indicate the presence of S as in Figure 1).

776 **Alt text:** Graphs showing the showing the concentration of water, carbon dioxide, and sulfur
777 or chi dissolved in the melt decreasing with decreasing pressure during closed-system
778 degassing for three different initial water concentrations of 0.2, 1, 3, and 5 weight percent. The
779 depth at which ten percent of water, sulfur, and chi has degassed is similar to the depth at which
780 ten percent water in the pure-water system would have degassed. The behaviour of sulfur and
781 chi is very similar.

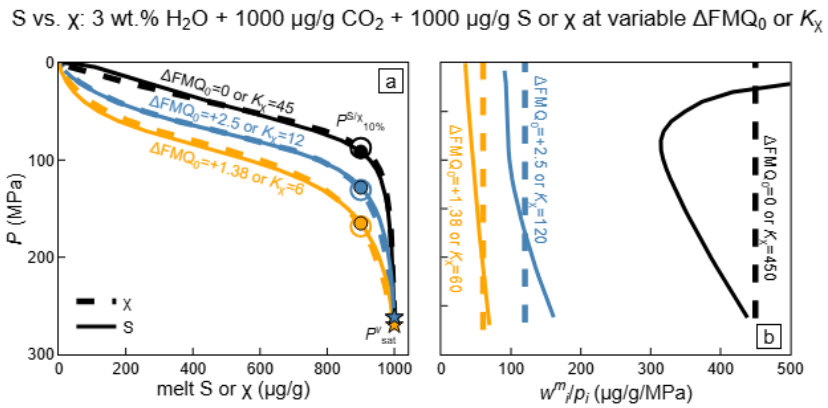

782

783 **Figure 4.** The effect of varying ΔFMQ_0 or K_χ during equilibrium, isothermal, decompression-
784 induced, closed-system degassing. The initial conditions are bulk concentrations of 3 wt.%
785 H_2O + 1000 µg/g CO_2 + 1000 µg/g S or χ at either varying ΔFMQ_0 for S or K_χ for χ (ΔFMQ_0=0),
786 where curve colour indicates ΔFMQ_0 or K_χ (µg/g/MPa): ΔFMQ_0=0 or K_χ=450 (black),
787 ΔFMQ_0+1.38 (SS^{min} where initial melt S^{6+}/S_T = 0.75) or K_χ=60 (yellow), and ΔFMQ_0+2.5 or
788 K_χ=120 blue); and curve style indicates S (solid) or χ (dash). **(a)** Concentration in the melt of
789 S or χ; and **(b)** w^m_i/p_j vs. P, which is an equilibrium constant (K_i, eq. 1) – for S, p_i is the sum of
790 p_{SO2} and p_{H2S}.

791 **Alt text:** Graphs comparing the behaviour of sulfur at different initial oxygen fugacities and
792 chi with different equilibrium constants that have been chosen to match the behaviour of sulfur
793 during degassing. Panel A shows the concentration of sulfur and chi decreasing very similarly
794 with decreasing pressure. Panel B shows the equilibrium constants for sulfur and chi with
795 pressure.

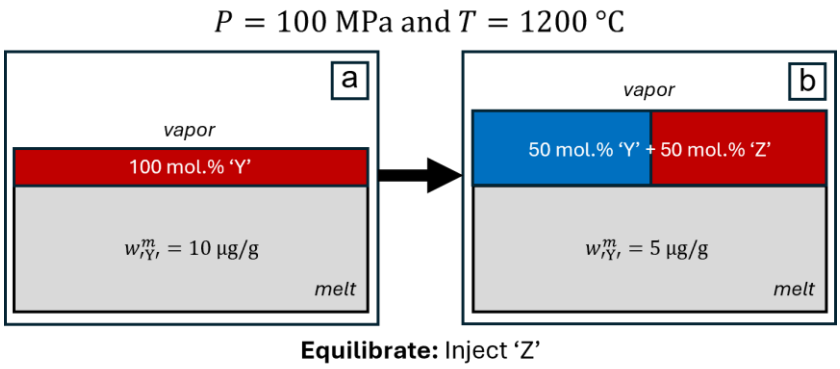

796

797 **Figure 5.** Schematic illustration of dilution driven degassing of a vapor-saturated silicate melt
798 by isobaric, isothermal addition of an insoluble volatile species into the system. **(a)** Initially, at
799 P = 100 MPa and T = 1200 °C, the vapor-saturated melt contains 10 µg/g of "Y" because the
800 vapor is pure "Y" (which is an ideal gas) and the equilibrium constant for "Y" ($K_{\text{"Y"}}$) is 0.1
801 µg/g/MPa. Component "Z", which is insoluble in the silicate melt, is added to the vapor in (a)
802 at constant P (100 MPa), until the vapor is 50 mol.% "Y" and 50 mol.% "Z", whilst "Y" is
803 equilibrating between the melt and vapor. **(b)** This means the vapor is now a 50:50 mol.% mix
804 of "Y" and "Z" and, to maintain equilibrium, "Y" has degassed until there is 5 µg/g in the melt.
805 The vapor volume has increased to maintain constant P as the number of moles in the vapor
806 has increased.

807 **Alt text:** Schematic illustration of changes in melt and vapor composition at constant pressure
808 and temperature when species Z is injected to a system only containing species Y. Panel A
809 shows the initial system containing 10 micro grams per gram of species Y dissolved in the melt
810 and a vapor of 100 mole percent species Y. Panel B shows the system after species Z has been
811 added, which now contains 5 micro grams per gram of species Y dissolved in the melt and a
812 vapor containing 50 mole percent of species Y and 50 mole percent of species Z.

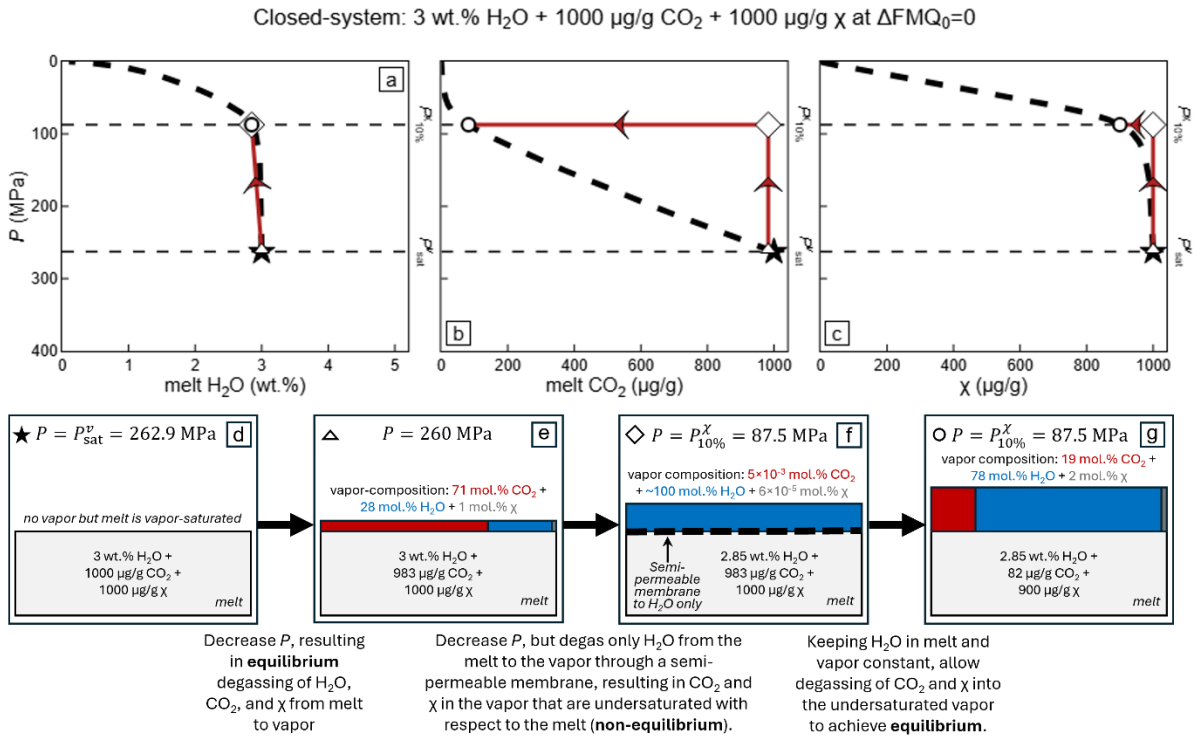

Figure 6. Degassing curves and schematic illustrations of the thought experiment described in the text illustrating the effect of dilution by H_2O on CO_2 and χ during isothermal, decompression-induced, closed-system degassing for initial conditions of 3 wt.% H_2O-eq + 1000 µg/g CO_2-eq + 1000 µg/g χ at ΔFMQ_0=0. The thick, black-dashed curves for **(a)** H_2O, **(b)** CO_2, and **(c)** χ show their concentrations during equilibrium degassing, which are reproduced from Figure 3. The schematic illustrations in **(d–g)** show the evolution after each step of the thought experiment of the concentrations in the melt of H_2O, CO_2, and χ (as indicated in the light grey boxes labelled "melt"); and the mol.% in the vapor of CO_2 (red), H_2O (blue), and χ (dark grey) written above the coloured boxes and by the areas of these coloured boxes, which are collectively indicatively proportional to the volume of vapor present in the system. **(d)** $P = P^v_{sat}$ = 262.9 MPa (filled star in a–c): although the melt is vapor saturated at this point, there is no vapor; **(e)** equilibrium degassing of H_2O, CO_2, and χ to P = 260.0 MPa (open triangle in a–c); **(f)** artificial degassing of only H_2O through a semi-permeable membrane to $P = P^{10\%}_{\chi}$ = 87.5 MPa with no degassing of CO_2 or χ (open diamond in a–c); and

(g) equilibration by degassing of CO_2 and χ without further H_2O degassing at $P = P^{10\%}{}_{\chi} = 87.5$ MPa (filled circle in a–c).

Alt text: Graphs and schematic illustration of changes in the melt and vapor composition during degassing. Panel A shows the concentration of water dissolved in the melt decreasing with decreasing pressure. Panel B shows the concentration of carbon dioxide dissolved in the melt decreasing with decreasing pressure. Panel C shows the concentration of chi dissolved in the melt with decreasing with decreasing pressure. Panel D shows the initial system at 262.9 MPa with all volatiles dissolved in the melt. Panel E shows the system at 260 MPa with a small amount of vapor after equilibrium degassing. Panel F shows the system at 87.5 MPa where only water has degassed into the vapor but carbon dioxide and chi are artificially retained in the melt and therefore highly diluted in the vapor. Panel G shows the system at 87.5 MPa at equilibrium, where carbon dioxide and chi have degassed from the melt to the vapor.

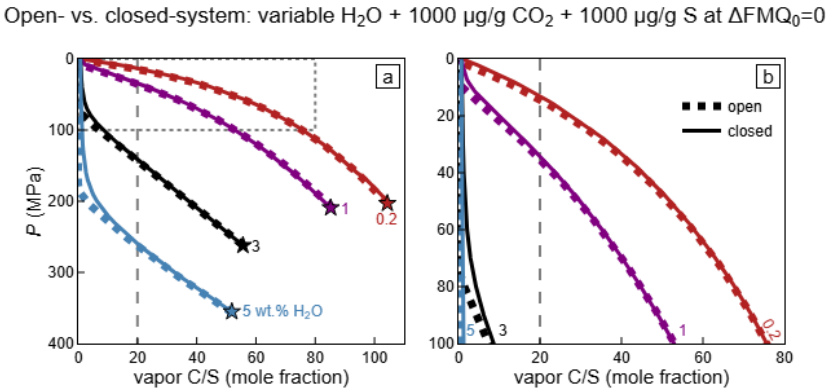

840

841 **Figure 7.** Effect of varying bulk H_2O on the C/S ratio of the vapor during equilibrium,
842 isothermal, decompression-induced, closed- and open-system degassing. The initial conditions
843 are bulk concentrations of variable H_2O + 1000 µg/g CO_2 + 1000 µg/g S at ΔFMQ_0=0. Curve
844 colours and styles as in Figure 1, with the addition of the vertical grey dashed line in (a) for
845 C/S = 20. The dotted box in (a) shows the extent of (b).

846 **Alt text:** Graphs showing decreasing carbon to sulfur ratio in the vapor with decreasing
847 pressure for different initial water concentrations in the melt for open- and closed-system
848 degassing. Panel B is a zoomed in version of panel A to highlight the behaviour at low
849 pressures.

References

Aiuppa, A., Bitetto, M., Francofonte, V., Velasquez, G., Parra, C. B., Giudice, G., Liuzzo, M., Moretti, R., Moussallam, Y., Peters, N., Tamburello, G., Valderrama, Oscar. A., & Curtis, A. (2017). A CO2-gas precursor to the March 2015 Villarrica volcano eruption. *Geochemistry, Geophysics, Geosystems*, *18*(6), 2120–2132. https://doi.org/10.1002/2017GC006892

Aiuppa, A., Moretti, R., Federico, C., Giudice, G., Gurrieri, S., Liuzzo, M., Papale, P., Shinohara, H., & Valenza, M. (2007). Forecasting Etna eruptions by real-time observation of volcanic gas composition. *Geology*, *35*(12), 1115–1118. https://doi.org/10.1130/G24149A.1

Anderson, A. T. J., Newman, S., Williams, S. N., Druitt, T. H., Skirius, C., & Stolper, E. M. (1989). H2O, CO2, CI, and gas in Plinian and ash-flow Bishop rhyolite. *Geology*, *17*(3), 221–225. https://doi.org/10.1130/0091-7613(1989)017

Anderson, A. T. J., & Wright, T. L. (1972). Phenocrysts and glass inclusions and their bearing on oxidation and mixing of basaltic magmas, kilauea volcano, hawaii. *American Mineralogist*, *57*(1–2), 188–216. https://pubs.geoscienceworld.org/msa/ammin/article-abstract/57/1-2/188/542575/Phenocrysts-and-glass-inclusions-and-their-bearing

Anderson, O. E., Jackson, M. G., Dottin, J., Harðardóttir, S., Koga, K. T., Seward, G., Cottle, J., Rose-Koga, E. F., & Gauer-Pasqualon, N. (2025). Volatiles in olivine-hosted melt inclusions from a rejuvenated O‘ahu tephra: Degree of melting controls the primary melt CO2 content—And extent of H2O degassing—Of OIB. *Chemical Geology*, *678*, 122604. https://doi.org/10.1016/J.CHEMGEO.2024.122604

Anderson, O. E., Jackson, M. G., Pamukçu, A. S., Rose-Koga, E. F., Le Roux, V., Klein, F., Koga, K. T., Gaetani, G. A., & Price, A. A. (2024). Extensive H2O degassing in deeply erupted submarine glasses inferred from Samoan melt inclusions: The EM2 mantle source is damp, not dry. *Chemical Geology*, *651*, 121979. https://doi.org/10.1016/J.CHEMGEO.2024.121979

Armstrong, L. S., Hirschmann, M. M., Stanley, B. D., Falksen, E. G., & Jacobsen, S. D. (2015). Speciation and solubility of reduced C-O-H-N volatiles in mafic melt: Implications for volcanism, atmospheric evolution, and deep volatile cycles in the terrestrial planets. *Geochimica et Cosmochimica Acta*, *171*, 283–302. https://doi.org/10.1016/j.gca.2015.07.007

Backnaes, L., & Deubener, J. (2011). Experimental studies on sulfur solubility in silicate melts at near-atmospheric pressure. *Reviews in Mineralogy and Geochemistry*, *73*, 143–165. https://doi.org/10.2138/rmg.2011.73.6

Baker, D. R., & Moretti, R. (2011). Modeling the Solubility of Sulfur in Magmas: A 50-Year Old Geochemical Challenge. *Reviews in Mineralogy and Geochemistry*, *73*(1), 167–213. https://doi.org/10.2138/RMG.2011.73.7

Baumgartner, R. J., Baratoux, D., Gaillard, F., & Fiorentini, M. L. (2017). Numerical modelling of erosion and assimilation of sulfur-rich substrate by martian lava flows: Implications for the genesis of massive sulfide mineralization on Mars. *Icarus*, *296*, 257–274. https://doi.org/10.1016/j.icarus.2017.06.016

Blundy, J., Mavrogenes, J., Tattitch, B., Sparks, S., & Gilmer, A. (2015). Generation of porphyry copper deposits by gas–brine reaction in volcanic arcs. *Nature Geoscience 2014 8:3*, *8*(3), 235–240. https://doi.org/10.1038/ngeo2351

Boulliung, J., & Wood, B. J. (2022). SO2 solubility and degassing behavior in silicate melts. *Geochimica et Cosmochimica Acta Volume , 1 November 2022, Pages 150-164*, *336*, 150–164. https://doi.org/10.1016/j.gca.2022.08.032

Boulliung, J., & Wood, B. J. (2023). Sulfur oxidation state and solubility in silicate melts. *Contributions to Mineralogy and Petrology*, *178*(8), 1–15. https://doi.org/10.1007/S00410-023-02033-9/FIGURES/9

Brounce, M. N., Kelley, K. A., Stern, R., Martinez, F., & Cottrell, E. (2016). The Fina Nagu volcanic complex: Unusual submarine arc volcanism in the rapidly deforming southern Mariana margin. *Geochemistry, Geophysics, Geosystems*, *17*(10), 4078–4091. https://doi.org/10.1002/2016GC006457

Brounce, M. N., Stolper, E. M., & Eiler, J. M. (2017). Redox variations in Mauna Kea lavas, the oxygen fugacity of the Hawaiian plume, and the role of volcanic gases in Earth's oxygenation. *Proceedings of the National Academy of Sciences of the United States of America*, *114*. https://doi.org/10.1073/pnas.1619527114

Burgisser, A., & Scaillet, B. (2007). Redox evolution of a degassing magma rising to the surface. *Nature*, *445*(7124), 194–197. https://doi.org/10.1038/nature05509

Burton, M. R., Allard, P., Murè, F., & La Spina, A. (2007). Magmatic gas composition reveals the source depth of slug-driven strombolian explosive activity. *Science (New York, N.Y.)*, *317*(5835), 227–230. https://doi.org/10.1126/science.1141900

Candela, P. A. (1986). The evolution of aqueous vapor from silicate melts: Effect on oxygen fugacity. *Geochimica et Cosmochimica Acta*, *50*(6), 1205–1211. https://doi.org/10.1016/0016-7037(86)90403-5

Carmichael, I. S. E., & Ghiorso, M. S. (1986). Oxidation-reduction relations in basic magma: a case for homogeneous equilibria. *Earth and Planetary Science Letters*, *78*(2–3), 200–210. https://doi.org/10.1016/0012-821X(86)90061-0

Carroll, M. R., & Rutherford, M. J. (1985). Sulfide and sulfate saturation in hydrous silicate melts. *Journal of Geophysical Research: Solid Earth*, *90*(S02), C601–C612. https://doi.org/10.1029/JB090IS02P0C601

Carroll, M. R., & Stolper, E. M. (1993). Noble gas solubilities in silicate melts and glasses: New experimental results for argon and the relationship between solubility and ionic porosity. *Geochimica et Cosmochimica Acta*, *57*(23–24), 5039–5051. https://doi.org/10.1016/0016-7037(93)90606-W

Cashman, K. V., & Blundy, J. D. (2000). Degassing and crystallization of ascending andesite and dacite. *Philosophical Transactions of the Royal Society A: Mathematical, Physical and Engineering Sciences*, *358*(1770), 1487–1513. https://doi.org/10.1098/rsta.2000.0600

Christopher, T., Edmonds, M., Humphreys, M. C. S., & Herd, R. A. (2010). Volcanic gas emissions from Soufrière Hills Volcano, Montserrat 1995-2009, with implications for mafic magma supply and degassing. *Geophysical Research Letters*, *37*(3). https://doi.org/10.1029/2009GL041325;ISSUE:ISSUE:DOI

Cicconi, M. R., Le Losq, C., Moretti, R., & Neuville, D. R. (2020). Magmas are the Largest Repositories and Carriers of Earth's Redox Processes. *Elements*, *16*(3), 173–178. https://doi.org/10.2138/GSELEMENTS.16.3.173

Cottrell, E., Birner, S. K., Brounce, M. N., Davis, F. A., Waters, L. E., & Kelley, K. A. (2021). Oxygen Fugacity Across Tectonic Settings. In R. Moretti & D. R. Neuville (Eds.), *Magma Redox Geochemistry* (pp. 33–61). American Geophysical Union (AGU). https://doi.org/10.1002/9781119473206.CH3

Cottrell, E., & Kelley, K. A. (2011). The oxidation state of Fe in MORB glasses and the oxygen fugacity of the upper mantle. *Earth and Planetary Science Letters*, *305*(3–4), 270–282. https://doi.org/10.1016/j.epsl.2011.03.014

Dalton, J. (1802). Essay IV. On the expansion of elastic fluids by heat. *Memoirs of the Literary and Philosophical Society of Manchester*, *5*(2), 595–602.

947 Davis, A. S., Clague, D. A., Schulz, M. S., & Hein, J. R. (1991). Low sulfur content in
948 submarine lavas: An unreliable indicator of subaerial eruption. *Geology*, *19*(7), 750–753.
949 https://doi.org/10.1130/0091-7613(1991)019<0750:LSCISL>2.3.CO;2
950 de Moor, J. M., Aiuppa, A., Avard, G., Wehrmann, H., Dunbar, N., Muller, C., Tamburello,
951 G., Giudice, G., Liuzzo, M., Moretti, R., Conde, V., & Galle, B. (2016). Turmoil at
952 Turrialba Volcano (Costa Rica): Degassing and eruptive processes inferred from high-
953 frequency gas monitoring. *Journal of Geophysical Research: Solid Earth*, *121*(8), 5761–
954 5775. https://doi.org/10.1002/2016JB013150
955 de Moor, J. M., Fischer, T. P., Sharp, Z. D., King, P. L., Wilke, M., Botcharnikov, R. E.,
956 Cottrell, E., Zelenski, M., Marty, B., Klimm, K., Rivard, C., Ayalew, D., Ramirez, C., &
957 Kelley, K. A. (2013). Sulfur degassing at Erta Ale (Ethiopia) and Masaya (Nicaragua)
958 volcanoes: Implications for degassing processes and oxygen fugacities of basaltic
959 systems. *Geochemistry, Geophysics, Geosystems*, *14*(10), 4076–4108.
960 https://doi.org/10.1002/ggge.20255
961 Di Muro, A., Pallister, J., Villemant, B., Newhall, C., Semet, M., Martinez, M., & Mariet, C.
962 (2008). Pre-1991 sulfur transfer between mafic injections and dacite magma in the Mt.
963 Pinatubo reservoir. *Journal of Volcanology and Geothermal Research*, *175*(4), 517–540.
964 https://doi.org/10.1016/J.JVOLGEORES.2008.02.025
965 Ding, S., Plank, T., de Moor, J. M., Moussallam, Y., Brounce, M., & Kelly, P. (2025).
966 Volcanic gases reflect magma stalling and launching depths. *Earth and Planetary*
967 *Science Letters*, *660*, 119349. https://doi.org/10.1016/j.epsl.2025.119349
968 Ding, S., Plank, T., Wallace, P. J., & Rasmussen, D. J. (2023). Sulfur_X: A Model of Sulfur
969 Degassing During Magma Ascent. *Geochemistry, Geophysics, Geosystems*, *24*(4),
970 e2022GC010552. https://doi.org/10.1029/2022GC010552
971 Dixon, J. E., Clague, D. A., & Stolper, E. M. (1991). Degassing History of Water, Sulfur, and
972 Carbon in Submarine Lavas from Kilauea Volcano, Hawaii. *The Journal of Geology*,
973 *99*(3), 371–394. https://doi.org/10.1086/629501
974 Dixon, J. E., & Stolper, E. M. (1995). An experimental study water and carbon dioxide
975 solubilities in mid-ocean ridge basaltic liquids. Part II: Application to degassing. *Journal*
976 *of Petrology*, *36*(6), 1633–1646.
977 Dixon, J. E., Stolper, E. M., & Holloway, J. R. (1995). An experimental study of water and
978 carbon dioxide solubilities in mid-ocean ridge basaltic liquids. Part I: Calibration and
979 solubility models. *Journal of Petrology*, *36*(6), 1607–1631.
980 https://doi.org/10.1093/oxfordjournals.petrology.a037267
981 Edmonds, M., Aiuppa, A., Humphreys, M., Moretti, R., Giudice, G., Martin, R. S., Herd, R.
982 A., & Christopher, T. (2010). Excess volatiles supplied by mingling of mafic magma at
983 an andesite arc volcano. *Geochemistry, Geophysics, Geosystems*, *11*(4).
984 https://doi.org/10.1029/2009GC002781;ISSUE:ISSUE:DOI
985 Edmonds, M., & Wallace, P. J. (2017). Volatiles and Exsolved Vapor in Volcanic Systems.
986 *Elements*, *13*(1), 29–34. https://doi.org/10.2113/gselements.13.1.29
987 Farsang, S., & Zajacz, Z. (2024). Sulfur species and gold transport in arc magmatic fluids.
988 *Nature Geoscience 2024 18:1*, *18*(1), 98–104. https://doi.org/10.1038/s41561-024-
989 01601-3
990 Fincham, C. J. B., & Richardson, F. D. (1954). The behaviour of sulphur in silicate and
991 aluminate melts. *Proceedings of the Royal Society of London. Series A. Mathematical*
992 *and Physical Sciences*, *223*(1152), 40–62. https://doi.org/10.1098/rspa.1954.0099
993 Frost, B. R. (1991). Introduction to oxygen fugacity and its petrologic importance. *Reviews in*
994 *Mineralogy and Geochemistry*, *25*, 1–9. https://ci.nii.ac.jp/naid/20001688380
995 Gaillard, F., Bernadou, F., Roskosz, M., Bouhifd, M. A., Marrocchi, Y., Iacono-Marziano,
996 G., Moreira, M., Scaillet, B., & Rogerie, G. (2022). Redox controls during magma ocean

997 degassing. *Earth and Planetary Science Letters*, *577*(6456), 117255.
998 https://doi.org/10.1016/j.epsl.2021.117255
999 Gaillard, F., Michalski, J., Berger, G., McLennan, S. M., & Scaillet, B. (2013). Geochemical
1000 reservoirs and timing of sulfur cycling on Mars. In *Space Science Reviews* (Vol. 174,
1001 Numbers 1–4, pp. 251–300). Springer. https://doi.org/10.1007/s11214-012-9947-4
1002 Gaillard, F., & Scaillet, B. (2009). The sulfur content of volcanic gases on Mars. *Earth and*
1003 *Planetary Science Letters*, *279*(1–2), 34–43.
1004 https://doi.org/10.1016/J.EPSL.2008.12.028
1005 Gaillard, F., & Scaillet, B. (2014). A theoretical framework for volcanic degassing chemistry
1006 in a comparative planetology perspective and implications for planetary atmospheres.
1007 *Earth and Planetary Science Letters*, *403*, 307–316.
1008 https://doi.org/10.1016/j.epsl.2014.07.009
1009 Gaillard, F., Scaillet, B., & Arndt, N. T. (2011). Atmospheric oxygenation caused by a
1010 change in volcanic degassing pressure. *Nature*, *478*(7368), 229–232.
1011 https://doi.org/10.1038/nature10460
1012 Gaillard, F., Scaillet, B., Pichavant, M., & Iacono-Marziano, G. (2015). The redox
1013 geodynamics linking basalts and their mantle sources through space and time. *Chemical*
1014 *Geology*, *418*, 217–233. https://doi.org/10.1016/j.chemgeo.2015.07.030
1015 Gerlach, T. M., & Thomas, D. M. (1986). Carbon and sulphur isotopic composition of
1016 Kilauea parental magma. *Nature*, *319*(6053), 480–483. https://doi.org/10.1038/319480a0
1017 Giggenbach, W. F. (1996). Chemical Composition of Volcanic Gases. *Monitoring and*
1018 *Mitigation of Volcano Hazards*, 221–256. https://doi.org/10.1007/978-3-642-80087-0_7
1019 Gonnermann, H. M., & Mukhopadhyay, S. (2007). Non-equilibrium degassing and a
1020 primordial source for helium in ocean-island volcanism. *Nature 2007 449:7165*,
1021 *449*(7165), 1037–1040. https://doi.org/10.1038/nature06240
1022 Hattori, K. H., & Keith, J. D. (2001). Contribution of mafic melt to porphyry copper
1023 mineralization: Evidence from Mount Pinatubo, Philippines, and Bingham Canyon,
1024 Utah, USA. *Mineralium Deposita*, *36*(8), 799–806.
1025 https://doi.org/10.1007/S001260100209/METRICS
1026 Herd, C. D. K., & Benaroya, S. (2025). Revisiting the oxygen fugacity of martian meteorites:
1027 implications for the redox history of the mantle of Mars. *Geochimica et Cosmochimica*
1028 *Acta*, *410*(6108), 121–140. https://doi.org/10.1016/j.gca.2025.10.001
1029 Hirschmann, M. M., Withers, A. C., Ardia, P., & Foley, N. T. (2012). Solubility of molecular
1030 hydrogen in silicate melts and consequences for volatile evolution of terrestrial planets.
1031 *Earth and Planetary Science Letters*, *345–348*, 38–48.
1032 https://doi.org/10.1016/J.EPSL.2012.06.031
1033 Holloway, J. R., & Blank, J. G. (1994). Application of experimental results to C-O-H species
1034 in natural melts. *Reviews in Mineralogy and Geochemistry1*, *30*, 187–230.
1035 Hughes, E. C., Ding, S., Iacovino, K., Wieser, P. E., & Kilgour, G. (2023). Workshop report:
1036 Modelling volatile behaviour in magmas. *Earth ArXiv*.
1037 https://doi.org/10.31223/X5FD3Q
1038 Hughes, E. C., Liggins, P., Saper, L., & Stolper, E. M. (2024). The effects of oxygen fugacity
1039 and sulfur on the pressure of vapor-saturation of magma. *American Mineralogist*, *109*,
1040 422–438.
1041 Hughes, E. C., Liggins, P., & Wieser, P. (2025). *ery-hughes/VolFe: VolFe*. Zenodo.
1042 Hughes, E. C., Liggins, P., Wieser, P., & Stolper, E. M. (2025). VolFe: an open-source
1043 Python package for calculating melt-vapour equilibria including silicate melt, carbon,
1044 hydrogen, sulfur, and noble gases. *Volcanica*, *8*(2), 457–-481.
1045 https://doi.org/10.30909/vol/imvc1781

Hughes, E. C., Saper, L. M., Liggins, P., O'Neill, H. St. C., & Stolper, E. M. (2023). The sulfur solubility minimum and maximum in silicate melt. *Journal of the Geological Society*, *180*, jgs2021-125. https://doi.org/https://doi.org/10.1144/jgs2021-125

Iacono-Marziano, G., Paonita, A., Rizzo, A., Scaillet, B., & Gaillard, F. (2010). Noble gas solubilities in silicate melts: New experimental results and a comprehensive model of the effects of liquid composition, temperature and pressure. *Chemical Geology*, *279*(3–4), 145–157. https://doi.org/10.1016/J.CHEMGEO.2010.10.017

Iacovino, K. (2015). Linking subsurface to surface degassing at active volcanoes: A thermodynamic model with applications to Erebus volcano. *Earth and Planetary Science Letters*, *431*, 59–74. https://doi.org/10.1016/J.EPSL.2015.09.016

Iacovino, K., Matthews, S., Wieser, P. E., Moore, G. M., & Bégué, F. (2021). VESIcal Part I: An open-source thermodynamic model engine for mixed volatile (O-) solubility in silicate melts. *Earth and Space Science*, e2020EA001584. https://doi.org/10.1029/2020EA001584

Katsura, T., & Nagashima, S. (1974). Solubility of sulfur in some magmas at 1 atmosphere. *Geochimica et Cosmochimica Acta*, *38*(4), 517–531. https://doi.org/10.1016/0016-7037(74)90038-6

Kern, C., Aiuppa, A., & de Moor, J. M. (2022). A golden era for volcanic gas geochemistry? *Bulletin of Volcanology 2022 84:5*, *84*(5), 1–11. https://doi.org/10.1007/S00445-022-01556-6

Lerner, A. H., Wallace, P. J., Shea, T., Mourey, A. J., Kelly, P. J., Nadeau, P. A., Elias, T., Kern, C., Clor, L. E., Gansecki, C., Lee, R. L., Moore, L. R., & Werner, C. A. (2021). The petrologic and degassing behavior of sulfur and other magmatic volatiles from the 2018 eruption of Kīlauea, Hawai'i: melt concentrations, magma storage depths, and magma recycling. *Bulletin of Volcanology*, *83*(6), 43. https://doi.org/10.1007/s00445-021-01459-y

Lesne, P., Scaillet, B., & Pichavant, M. (2015). The solubility of sulfur in hydrous basaltic melts. *Chemical Geology*, *418*, 104–116. https://doi.org/10.1016/J.CHEMGEO.2015.03.025

Liggins, P. (2023). EVo: Thermodynamic magma degassing model. *Astrophysics Source Code Library*, ascl:2307.052. https://ui.adsabs.harvard.edu/abs/2023ascl.soft07052L/abstract

Liggins, P., Jordan, S., Rimmer, P. B., & Shorttle, O. (2022). Growth and Evolution of Secondary Volcanic Atmospheres: I. Identifying the Geological Character of Hot Rocky Planets. *Journal of Geophysical Research: Planets*, *127*(7), e2021JE007123. https://doi.org/10.1029/2021JE007123

Liggins, P., Shorttle, O., & Rimmer, P. B. (2020). Can volcanism build hydrogen-rich early atmospheres? *Earth and Planetary Science Letters*, *550*, 116546. https://doi.org/10.1016/J.EPSL.2020.116546

Lo, M., La Spina, G., Joy, K. H., Polacci, M., & Burton, M. (2021). Determining the Effect of Varying Magmatic Volatile Content on Lunar Magma Ascent Dynamics. *Journal of Geophysical Research: Planets*, *126*(11), e2021JE006939. https://doi.org/10.1029/2021JE006939

Lowenstern, J. B. (1995). Applications of silicate-melt inclusions to the study of magmatic volatiles. In J. F. H. Thompson (Ed.), *Magmas, fluids and ore deposits. Mineralogical Assoication of Canada Short Course Volume no.23* (pp. 71–99).

Lowenstern, J. B. (2001). Carbon dioxide in magmas and implications for hydrothermal systems. *Mineralium Deposita*, *36*(6), 490–502. https://doi.org/10.1007/S001260100185/METRICS

Mathez, E. A. (1984). Influence of degassing on oxidation states of basaltic magmas. *Nature*, *310*(5976), 371–375. https://doi.org/10.1038/310371a0

Matjuschkin, V., Blundy, J. D., & Brooker, R. A. (2016). The effect of pressure on sulphur speciation in mid- to deep-crustal arc magmas and implications for the formation of porphyry copper deposits. *Contributions to Mineralogy and Petrology*, *171*(7), 66. https://doi.org/10.1007/s00410-016-1274-4

Métrich, N., Berry, A. J., O'Neill, H. St. C., & Susini, J. (2009). The oxidation state of sulfur in synthetic and natural glasses determined by X-ray absorption spectroscopy. *Geochimica et Cosmochimica Acta*, *73*(8), 2382–2399. https://doi.org/10.1016/J.GCA.2009.01.025

Metrich, N., & Mandeville, C. W. (2010). Sulfur in Magmas. *Elements*, *6*(2), 81–86. https://doi.org/10.2113/gselements.6.2.81

Métrich, N., & Wallace, P. J. (2009). Volatile Abundances in Basaltic Magmas and Their Degassing Paths Tracked by Melt Inclusions. *Reviews in Mineralogy and Geochemistry*, *69*(1). http://rimg.geoscienceworld.org/content/69/1/363

Moore, J. G., & Clague, D. (1987). Coastal lava flows from Mauna Loa and Hualalai volcanoes, Kona, Hawaii. *Bulletin of Volcanology*, *49*(6), 752–764. https://doi.org/10.1007/BF01079826

Moore, J. G., & Fabbi, B. P. (1971). An estimate of the juvenile sulfur content of basalt. *Contributions to Mineralogy and Petrology*, *33*(2), 118–127. https://doi.org/10.1007/BF00386110

Moore, J. G., & Schilling, J.-G. (1973). Vesicles, water, and sulfur in Reykjanes Ridge basalts. *Contributions to Mineralogy and Petrology*, *41*(2), 105–118. https://doi.org/10.1007/BF00375036

Moore, J. G., & Thomas, D. M. (1988). Subsidence of Puna, Hawaii inferred from sulfur content of drilled lava flows. *Journal of Volcanology and Geothermal Research*, *35*(1–2), 165–171. https://doi.org/10.1016/0377-0273(88)90013-3

Moretti, R. (2021). Ionic Syntax and Equilibrium Approach to Redox Exchanges in Melts: Basic Concepts and the Case of Iron and Sulfur in Degassing Magmas. In R. Moretti & D. R. Neuville (Eds.), *Magma Redox Geochemistry, Geophysical Monograph Series* (1st ed., pp. 115–138). American Geophysical Union (AGU). https://doi.org/10.1002/9781119473206.CH6

Moretti, R., & Ottonello, G. (2003). Polymerization and disproportionation of iron and sulfur in silicate melts: Insights from an optical basicity-based approach. *Journal of Non-Crystalline Solids*, *323*(1–3), 111–119. https://doi.org/10.1016/S0022-3093(03)00297-7

Moretti, R., & Ottonello, G. (2005). Solubility and speciation of sulfur in silicate melts: The Conjugated Toop-Samis-Flood-Grjotheim (CTSFG) model. *Geochimica et Cosmochimica Acta*, *69*(4), 801–823. https://doi.org/10.1016/J.GCA.2004.09.006

Moretti, R., Papale, P., & Ottonello, G. (2003). A model for the saturation of C-O-H-S fluids in silicate melts. *Geological Society, London, Special Publications*, *213*(1), 81–101. https://doi.org/10.1144/GSL.SP.2003.213.01.06

Moussallam, Y., Edmonds, M., Scaillet, B., Peters, N., Gennaro, M. E., Sides, I., & Oppenheimer, C. (2016). The impact of degassing on the oxidation state of basaltic magmas: A case study of Kīlauea volcano. *Earth and Planetary Science Letters*, *450*, 317–325. https://doi.org/10.1016/j.epsl.2016.06.031

Moussallam, Y., Oppenheimer, C., Scaillet, B., Gaillard, F., Kyle, P., Peters, N., Hartley, M. E., Berlo, K., & Donovan, A. (2014). Tracking the changing oxidation state of Erebus magmas, from mantle to surface, driven by magma ascent and degassing. *Earth and Planetary Science Letters*, *393*, 200–209. https://doi.org/10.1016/j.epsl.2014.02.055

Nash, W. M., Smythe, D. J., & Wood, B. J. (2019). Compositional and temperature effects on sulfur speciation and solubility in silicate melts. *Earth and Planetary Science Letters*, *507*, 187–198. https://doi.org/10.1016/J.EPSL.2018.12.006

Nilsson, K., & Peach, C. L. (1993). Sulfur speciation, oxidation state, and sulfur concentration in backarc magmas. *Geochimica et Cosmochimica Acta*, *57*(15), 3807–3813. https://doi.org/10.1016/0016-7037(93)90158-S

O'Neill, H. St. C. (2021). The thermodynamic controls on sulfide saturation in silicate melts with application to Ocean Floor Basalts. In R. Moretti & D. R. Neuville (Eds.), *Magma Redox Geochemistry, Geophysical Monograph Series* (pp. 177–213). John Wiley & Sons, Inc. https://doi.org/10.1002/9781119473206.ch10

O'Neill, H. St. C., & Mavrogenes, J. A. (2002). The sulfide capacity and the sulfur content at sulfide saturation of silicate melts at 1400°C and 1 bar. *Journal of Petrology*, *43*(6), 1049–1087. https://doi.org/10.1093/petrology/43.6.1049

O'Neill, H. St. C., & Mavrogenes, J. A. (2022). The sulfate capacities of silicate melts. *Geochimica et Cosmochimica Acta*. https://doi.org/10.1016/J.GCA.2022.06.020

Pallister, J. S., Hoblitt, R. P., & Reyes, A. G. (1992). A basalt trigger for the 1991 eruptions of Pinatubo volcano? *Nature 1992 356:6368*, *356*(6368), 426–428. https://doi.org/10.1038/356426a0

Papale, P., Moretti, R., & Paonita, A. (2022). Thermodynamics of Multi-component Gas–Melt Equilibrium in Magmas: Theory, Models, and Applications. *Reviews in Mineralogy and Geochemistry*, *87*(1), 431–556. https://doi.org/10.2138/RMG.2022.87.10

Plank, T., Kelley, K. A., Zimmer, M. M., Hauri, E. H., & Wallace, P. J. (2013). Why do mafic arc magmas contain ~4 wt% water on average? *Earth and Planetary Science Letters*, *364*(2), 168–179. https://doi.org/10.1016/j.epsl.2012.11.044

Rasmussen, D. J., Plank, T. A., Roman, D. C., & Zimmer, M. M. (2022). Magmatic water content controls the pre-eruptive depth of arc magmas. *Science*, *375*(6585), 1169–1172. https://doi.org/10.1126/science.abm5174

Rasmussen, D. J., Plank, T. A., Wallace, P. J., Newcombe, M. E., & Lowenstern, J. B. (2020). Vapor-bubble growth in olivine-hosted melt inclusions. *American Mineralogist*, *105*(12), 1898–1919. https://doi.org/10.2138/am-2020-7377

Roberge, J., Delgado-Granados, H., & Wallace, P. J. (2009). Mafic magma recharge supplies high CO2 and SO2 gas fluxes from Popocatépetl volcano, Mexico. *Geology*, *37*(2), 107–110. https://doi.org/10.1130/G25242A.1

Seaman, C., Sherman, S. B., Garcia, M. O., Baker, M. B., Balta, B., & Stolper, E. (2004). Volatiles in glasses from the HSDP2 drill core. *Geochemistry, Geophysics, Geosystems*, *5*(9), 9–16. https://doi.org/10.1029/2003GC000596

Stolper, E. M. (1982). The speciation of water in silicate melts. *Geochimica et Cosmochimica Acta*, *46*(12), 2609–2620. http://www.sciencedirect.com/science/article/pii/0016703782903817

Symonds, R. B., Rose, W. I., Bluth, G. J. S., & Gerlach, T. M. (1994). Volcanic-gas studies: methods, results, and applications. In M. R. Carroll & J. R. Holloway (Eds.), *Volatiles in Magmas* (pp. 1–66).

Thomas, R. W., & Wood, B. J. (2022). The effect of composition on chlorine solubility and behaviour in silicate melts. *American Mineralogist*. http://www.minsocam.org/msa/ammin/AM_Preprints/8450WoodPreprint.pdf

Verhoogen J. (1949). *Thermodynamics of a magmatic gas phase*. University of California Press.

Wallace, P. J. (2001). Volcanic SO2 emissions and the abundance and distribution of exsolved gas in magma bodies. *Journal of Volcanology and Geothermal Research*, *108*(1–4), 85–106. https://doi.org/10.1016/S0377-0273(00)00279-1

Wallace, P. J. (2005). Volatiles in subduction zone magmas: concentrations and fluxes based on melt inclusion and volcanic gas data. *Journal of Volcanology and Geothermal Research*, *140*(1–3), 217–240. https://doi.org/10.1016/j.jvolgeores.2004.07.023

Wallace, P. J., & Carmichael, I. S. E. (1992). Sulfur in basaltic magmas. *Geochimica et Cosmochimica Acta*, *56*(5), 1863–1874. https://doi.org/10.1016/0016-7037(92)90316-B

Wallace, P. J., & Carmichael, I. S. E. (1994). S speciation in submarine basaltic glasses as determined by measurements of SKa X-ray wavelength shifts. *American Mineralogist*, *79*, 161–167.

Wallace, P. J., & Edmonds, M. (2011). The Sulfur Budget in Magmas: Evidence from Melt Inclusions, Submarine Glasses, and Volcanic Gas Emissions. *Reviews in Mineralogy and Geochemistry*, *73*(1), 215–246. https://doi.org/10.2138/rmg.2011.73.8

Wallace, P. J., Plank, T., Edmonds, M., & Hauri, E. H. (2015). Volatiles in Magmas. *The Encyclopedia of Volcanoes*, 163–183. https://doi.org/10.1016/B978-0-12-385938-9.00007-9

Webster, J. D., & Botcharnikov, R. E. (2011). Distribution of sulfur between melt and fluid in S-O-H-C-Cl-bearing magmatic systems at shallow crustal pressures and temperatures. *Reviews in Mineralogy and Geochemistry*, *73*(1), 247–283. https://doi.org/10.2138/rmg.2011.73.9

Whitney, J. A. (1984). Fugacities of sulfurous gases in pyrrhotite-bearing silicic magma. *American Mineralogist*, *69*(1–2), 68–78. https://pubs.geoscienceworld.org/msa/ammin/article/69/1-2/68/41577/fugacities-of-sulfurous-gases-in-pyrrhotite

Wieser, P. E., Shi, S. C., Gleeson, M. L. M., Rangel, B., DeVitre, C. L., Bearden, A. T., Lynn, K. J., & Camille-Caumon, M. (2025). Fluid inclusion constraints on the geometry of the magmatic plumbing system beneath Mauna Loa — Part 1:lavas and tephras. *Bulletin of Volcanology 2025 87:10*, *87*(10), 89-. https://doi.org/10.1007/s00445-025-01874-5

Yip, S. T. H., Biggs, J., Edmonds, M., Liggins, P., & Shorttle, O. (2022). Contrasting Volcanic Deformation in Arc and Ocean Island Settings Due To Exsolution of Magmatic Water. *Geochemistry, Geophysics, Geosystems*, *23*(7), e2022GC010387. https://doi.org/10.1029/2022GC010387

Zajacz, Z., Candela, P. A., Piccoli, P. M., & Sanchez-Valle, C. (2012). The partitioning of sulfur and chlorine between andesite melts and magmatic volatiles and the exchange coefficients of major cations. *Geochimica et Cosmochimica Acta*, *89*, 81–101. https://doi.org/10.1016/J.GCA.2012.04.039